DEGRADATION OF COLD OPTICAL SYSTEMS BY CRYODEPOSITION. REPORT FOR 1971 INDEPENDENT RESEARCH PROGRAM

C. K. Liu

Lockheed Missiles and Space Company, Incorporated
Palo Alto, California

5 February 1972

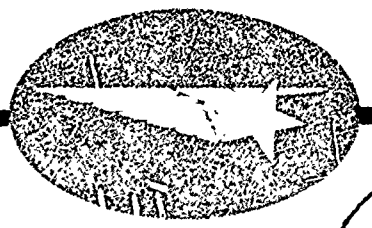

LMSC/D266319

5 Feb. 1972

TP-3347

DEGRADATION OF COLD OPTICAL SYSTEMS BY CRYODEPOSITION

REPORT FOR 1971
INDEPENDENT RESEARCH PROGRAM

BY
C. K. LIU

C. K. Liu
Member, Thermophysics
Infrared Programs
Engineering Sciences Laboratory

APPROVED: _____

M. McCargo
Member, Thermophysics
Infrared Programs
Engineering Sciences Lab.

CONTENTS

LIST OF FIGURES

LIST OF FIGURES

LIST OF TABLES

NOMENCLATURE

C	Condensation coefficient or capture coefficient; C_w is C of wall and C_c is C of cold optical surface
C_t	Transfer coefficient
E	Energy of gas molecules
e_b	Blackbody emission power
k	Boltzmann's consdtant = 1.38×10^{-6} erg/degree
k	Absorption index
L	Physical thickness
M	Molecular weight
N	Density of Molecules (cm^{-3}) = p/kT
N_m	Monolayer number density of condensed molecules, cm^{-2}
N_o	Avogadro's number = 6.02×10^{23}
$\bar{n}$	Complex index of refraction = $n - ik$
n	Molecule flux, cm^{-2} sec^{-1}
p	Pressure
Q	Heat of absorption
R	Gas constant, 1.987 cal/degree
T	Temperature
t	Optical depth defined by $\int_o^y \beta \, dy$
t_o	t when y = L
V_m	Maxwellian mean velocity of molecules = $2(2kTN_o/\pi M)^{1/2}$
V_s	Spacecraft velocity
W	Albedo parameter, $\sigma/(\sigma + \alpha)$

Greek Symbols

α	Absorption coefficient = $4\pi k/\lambda$
β	Exteinction coefficient, $\sigma + \alpha$
φ	Angle of reflection, view angle
λ	Wavelength
μ	Cos φ
$\rho_{ha}(\mu_1)$	Hemispherical-angular reflectance
$\rho_{ah}(\mu_1)$	Angular-hemispherical reflectance
ρ_{ba}	Biangular reflectance
ρ_{ba}^{d}	Diffuse component of a biangular reflectance
σ	Scattering coefficient
τ	Thickness of cryodeposit, time of adsorption
$\dot{\tau}$	Deposition rate
τ_o	Constant in Equation 2.2
ϕ	Azimuthal reflection angle
Ψ	Angle of incidence
ω	Solid angle

Subscript

1	Refers to vacuum
2	Refers to deposit
3	Refers to substrate

1971 INDEPENDENT RESEARCH REPORT - DEGRADATION OF COOLED OPTICAL SYSTEMS BY CRYODEPOSITION

1. INTRODUCTION

The work reported here represents the first year effort on one part of a three-year research program dealing with transient degradation and contamination of optical materials on orbiting spacecrafts. Present investigation concernted itself with the degradation of the optical system performance as a result of decreased transmission, scattering of out-of-field energy, decreased reflectance of mirrors and increased reflectance of "black" surfaces caused by the cryodeposition of condensible gases and the debris cloud formed by particulate and gaseous constituents. During the first year pertinent information have been collected to identify the possible contaminants associated with the spacecraft environment. A study has been conducted for the radiative characteristics of solid cryodeposit on transparent and opaque substrate. A distinction is made here between a cryodeposit and physically adsorbed gas. A cryodeposit forms when a condensible gas impinges on a cold surface and forms a solid deposit. Physical adsorption occurs when gas molecules impinge on a surface and remain, but without forming a crystalline deposit. Cryodeposition tests have also been conducted with specific contaminants to determine the degradation of a sensor performance.

The results of the present investigation are also applicable to the operation of

space simulation chambers using cryogenically cooled black panels; design of cryogenic storage tanks for long-time storage of cryogenic fluids in space; and the design on various thermal control surfaces of a spacecraft.

2. SOURCE OF CONTAMINANTS

The main source of contaminants that can cause contamination troubles on cooled optical surfaces of a spacecraft are the condensible gas constituents in the cloud of debris that accompanies the vehicle in space. This debris cloud is formed by (a) combustion product in reaction control system thruster firing; (b) outgassing, evaporation and sublimation of organic materials; and (c) waste removal, fuel leakage and systems venting products. The Angstrom size molecules cause absorption and Rayleigh scattering of solar irradiance. Among the micron size particles, the ice crystals contribute to scattering (where Mie theory applies) and the dust particles possessing high absorption coefficients contribute to light absorption. The dispersal of reflected light will elevate the background radiance and will interfere with the sensor operation if it exceeds the existing natural brightness magnitude (zodiacal light) significantly. Deposition of absorbing particles on the optical surfaces will change the radiative characteristics of the critical optical elements. These two kinds of contaminants may differ in physical characteristics and in their effects, but are almost equally detrimental. The net result is the collection of misleading data. Following discussions will be limited to sources of contaminants in cryodeposition only. The bakeground problem will be treated separately in future programs.

2.1 Combustion Products

The contamination effect of exhaust plumes on thermal control surfaces have been well documented in some recent studies (Ref. 1 and 2). It has also been reported that cryodeposition is probable from interaction between rocket and thruster exhaust product and cold optical surfaces (Ref. 3). This is evidenced by the unsatisfactory temperature control of the Nimbus II and III High Resolution Infrared Radiometer (HRIR) detector cells. These cells were designed to operate between 193 to 203°K. The initial values were close to the design point (Ref. 4). After a few hundred orbits, the cell temperature rose to greater than 208°K (Ref. 4, 5 and 6). As a result, the instrument noise to signal ratios were almost tripled. The situation may become worse as detector temperatures as low as 100 and 70°K are being considered for future ATS (Ref. 7) and SMS experiments (Ref. 8). At high vacuum, the exhaust gases form broad and expansive plumes resulting in impingement on spacecraft components far off the plume centerline.

The combustion products of the reaction control system thrusters used in the ATM service module and lunar module has been calculated (Ref. 9) and is given as a function of oxidizer/fuel ratio in Table 1. The oxidizer is N_2O_4 and the fuel is Aerozine 50 (50% UDMH + 50% hydrozine). Table 2 gives the combustion products of a R-4D engine used in the Skylab-configuration reaction control system with a N_2O_4/MMH propellant system (Ref. 10) Both computations are based on frozen equilibrium at entrance to the nozzle.

TABLE 1

COMBUSION PRODUCT OF N_2O_4 AND AEROZINE 50
IN MOLE FRACTION
(REF. 9)

O/F Ratio	1.4	2.0	2.2
N_2	0.32	0.331	0.332
CO	0.108	0.072	0.061
H_2O	0.319	0.368	0.367
H_2	0.19	0.073	0.055
CO_2	0.026	0.049	0.055
O	0	0.008	0.01
H	0.02	0.024	0.02
NO	0.0016	0.01	0.014
OH	0.012	0.045	0.051
O_2	0	0.018	0.03

TABLE 2

COMBUSION PRODUCT OF N_2O_4 AND MMH IN MOLE FRACTION (REF. 10)

O/F Ratio	1.24	2.17	3.07
CO	0.15345	0.07754	0
CO_2	0.02404	0.08144	0.1427
H	0.00256	0.01255	0
H_2	0.28853	0.05766	0
H_2O	0.24250	0.40147	0.42815
NO	.00002	0.00462	0.00014
N_2	.28857	0.32940	0.35705
O	0	0.0032	0
OH	.00032	0.02301	0.00004
O_2	0	0.00912	0.0719

When the molecular weights are small and vapor pressures are high, the deposited molecules will evaporate rather rapidly off the surfaces. Fig. 1 shows the vapor pressures at low temperatures of various gases (Ref. 11). It can be seen that among the combustion products of the thrusters, CO_2 and H_2O molecules are most likely to deposit on cold surfaces at the space environment of high vacuum.

2.2 Spacecraft Outgassing

The main sources of high molecular weight contaminants on a spacecraft originate from outgassing, evaporation and sublimation from organic materials like adhesives, epoxies, paints and coatings. The outgassing rate is usually represented by a weight loss versus time curve. For a polymerical material in vacuum, the early weight losses consist mainly of occluded and adsorbed gases and solvents. Those that sublimate more slowly are the plastisizers, incompletely polymerized fragments, thermally unraveled fragments, photon-induced decomposition products, additives, and other miscellaneous components acquired in the manufacturing or processing of the material. The time required for the material to reach its stationary-state weight loss rate is a function of the materia_ thickness and may be anything from 20 to several hundred hours for different materials. Experimental data given in Ref. 9 on outgassing rates of the surface materials associated with the ATM module components indicated that the adhesives and epoxies experience a greater initial weight loss and require a longer vacuum exposure time to attain steady-state equilibrium than do the paints and coatings.

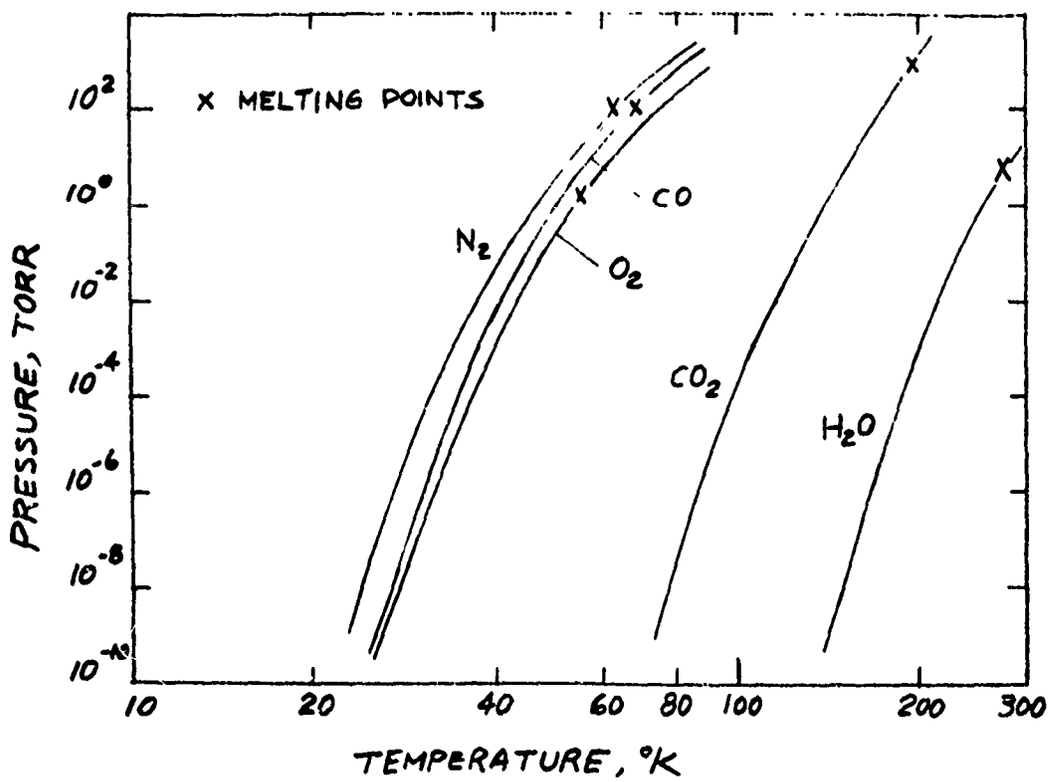

Fig. 1 Vapor Pressure versus Temperature (Ref. 11)

Even with the weight loss data known, the knowledge of the condensible fraction is necessary for any judgment of its potential threat. The number of molecules bombarding each square centimeter per second is

$$n = \frac{1}{4} N V_m = 3.52 \times 10^{22} \, p(MT)^{-1/2} \tag{2.1}$$

where N is the density of molecules, V_m the Maxwellian mean velocity, p the gas pressure in Torr, M the gas molecular weight and T the gas temperature in ^{o}K. The time of adsorption (sitting time) is given by the Frenkel equation

$$\tau = \tau_o \exp(Q/RT) \tag{2.2}$$

where Q is the heat of adsorption in cal/mole. The constant τ_o is period of the lattice vibrations of the solid surface and is generally of the order of 10^{-13}. The gas constant R is equal to 1.987 cal/degree. The number of molecules condensed per square centimeter on the solid is then given by

$$N = 3.52 \times 10^{22} \, p \, (MT)^{-1/2} \cdot \tau \cdot C \tag{2.3}$$

The coefficient C is defined as the fraction of the collisions that the molecules are trapped. If the solid has the same molecules as the gas, C is called "condensation coefficient." If the solid has molecules different from that of the gas, C is called "capture coefficient" or "sticking coefficient." Values of C depends on surface temperature, the flux density n, the thickness of the condensed phase, as well as the gas temperature and the angle of incidence. Temperature effect on values of C is given in Ref. 12. It shows that C decreases with increasing gas temperature, but increase with decreas-

ing surface temperature. Brown & Wang (Ref. 13) determined C of eleven common gases at 300°K on 77°K cryosurfaces. They found that the higher the molecular weight and heat of condensation, the higher the capture coefficient. More recent data on C can be found in Ref. 14. The values of C can also be determined by its relation with the mean energy accommodation coefficient $\bar{\alpha}$, when multiple collision is neglected. This is given by (Ref. 15).

$$\bar{\alpha} = C\alpha + (1-C)\,\alpha^{*} \tag{2.4}$$

where α is the accommodation coefficient for molecules that have condensed (become adsorbed) and α^{*} for molecules that have reflected. α is defined by

$$\alpha = \frac{E_i - E_r}{E_i - E_s} \tag{2.5}$$

where E_i is the mean energy of gas molecules impinging on the surface of a solid whose temperature is T_s; E_r the mean energy of the reflected gas molecules and E_s the mean energy of gas molecules at T_s. Values of α for some gases can be found in Ref. 16.

From the present limited knowledge of sublimated materials about a spacecraft, it is difficult to make a quantitative judgment about the contamination threat on cold optical systems. The known facts indicate that serious contamination buildup could occur from paint outgassing and result in degradation of the radiative characteristics of cold critical optical elements.

2.3 Overboard Discharge and Leakage

In a manned spacecraft, there are four principal groups of materials involved in the overboard discharge and leaks. These are water and urine, oxygen, hydrogen and propellants. It is more convenient to treat the effects of each group of material individually regardless of the source.

When liquid water or urine is dischraged through the vent and exposed to space vacuum, a sufficient amount will evaporate and the remainder will be frozen and reduced to its equilibrium temperature. This venting is the major contributor of particulate debris. Emission of oxygen from the spacecraft is due to leakage from pressurized habitation area and purging of fuel cells. In order to maintain efficient fuel cell operation, the impurities accumulated in the fuel cell can be periodically removed by purging with oxygen. The source of hydrogen discharge is from venting or leakage of the AgO/Zn batteries and the fuel cell hydrogen purge. These molecular species emanated from the spacecraft causes a background problem, but its contribution to cryocontamination will be very small.

Certain background leakage rate is expected through the propellant valves of various reaction control systems. These propellants could be troublesome contaminants. Calculations in Ref. 9 showed that the total leakage rate is in the order of 0.28 mg/sec in the ATM experiment.

3. RADIATIVE CHARACTERISTICS OF CRYODEPOSITS

The present section will be divided into three parts. The first part deals with the formation of cryodeposits from potential sources of contamination in the cooled optical system. The second part considers theoretical analyses on change of radiative characteristics of the optical surfaces due to the formation of cryodeposits. The final part reviews existing experimental data on H_2O and CO_2 cryodeposits taken in the past decade.

3.1 Formation of Cryodeposits

The rate of formation of a solid film on the cold optical surface from cryodeposition depends on the condensible constituents in the debris clouds; the rate of collision of these constituents with the exposed cold optical surfaces; and the capture coefficient of these constituents with respect to various optical surfaces.

The quantity of some condensible constituents in the debris cloud may be extimated from a given spacecraft in orbits of known missions. These include the contributions from combustion products of various thrusters, overboard discharges and leakages. Some weight loss data are also available on certain spacecraft materials but the information on its condensible constituents is still insufficient. For the present study only the molecules of CO_2 and H_2O will be considered.

The rate of collision of these molecules with respect to the cold optical surfaces can be calculated from equation (2.1). It depends only on the energy (temperature), pressure and molecular weight of the gas molecules. In a spacecraft sensor system, a forebaffle or sun shade is often required ahead of the sensor entrance aperture in order to reduce the incidence of out-of-field stray radiation on the entrance aperture. The number of molecules entering a sensor entrance aperture then depends on the orientation of the aperture with respect to the vehicle velocity vector. When the sensor entrance surface normal has a component along the velocity vector, some ambient molecules will be "scooped" up. In the extreme case where the velocity vector is normal to the entrance plane so that the maximum amount of scooping occurs, the number of molecules entering the entrance due to scooping will be

$$n = N \cdot V_s \ cm^{-2} \ sec^{-1} \qquad (3.1)$$

where V_s is the spacecraft velocity (cm/sec). Therefore, the ratio of this flux to the flux of Eq. (2.1) is $4 V_s/V_m$ and varies with the spacecraft velocity and the gas temperature. The maximum "scoop" deposition rate for given gas molecules will increase by four times if the vehicle velocity equals the mean molecular velocity.

If the sensor is viewing normal to the velocity vector and free molecular flow prevails, the molecules entering the baffle entrance will proceed in a straight line until they collide with the baffle wall, the first optical surface or any support structure in their way. If it is further assumed that the reflection of gas molecules at the surfaces is diffuse, the number of

molecules reaching the first cold optical surface can be determined in the same manner as for the amount of stray light reaching it after reflection from the baffle wall. The baffle entrance is a diffuse source and the baffle wall with the capture coefficient C_w has a diffuse reflection coefficient of $(1-C_w)$. The fraction of the source radiation that reaches the first cold optical surface either directly or after diffuse reflection from the baffle wall is defined as transfer coefficient, C_t. The mean flux density of molecules deposited on the first cold optical surface with capture coefficient C_c is then

$$\dot{n} = 3.52 \times 10^{22} \, p \cdot C_c \cdot C_t \, (MT)^{-1/2} \quad cm^{-2} \, sec^{-1} \tag{3.2}$$

Values of C_t as a function of $(1-C_w)$ have been calculated in Ref. 17 for a typical high performance sensor. If the monolayer number density is N_m molecules/cm^2, the rate of growth of the cryodeposit is then

$$\tau = \dot{n} \, (N_m)^{-3/2} \quad cm/sec \tag{3.3}$$

where N_m is of the order of 10^{15}.

3.2 Previous Analytical Work

Vast progress has been made in the analysis of radiative characteristics of solid films on various substrates. However, most of the results from the analytical investigation dealing with the radiant heat transfer in an absorbing, emitting and scattering medium were for high temperature application and for low values of the albedo parameter, W. The case of an isothermal dielectric film on a conducting substrate was investigated in Ref. 18. The

dielectric film was assumed to be infinite in extent but with finite thickness. The interfaces were assumed to be parallel and smooth with specular reflectance given by Fresnel's law. Closed form analytical solutions were obtained when scattering was neglected. Similar non-scattering analysis was performed for ice cryodeposits (Ref. 19). Since scattering is not prominent for H_2O deposits in the infrared region which was considered, the agreement between analytical and experimental results was reasonable.

When scattering is accounted for the analyses have been primarily of a high temperature nature. The classical method of discrete cooredinate has been used (Ref. 20 and 21) to approximate the equation of radiative transport. The resulting system of simultaneous ordinary differential equations was solved by finding the eigen-values and eigen-vectors. Generally, convergence of the resulting computer program could not be obtained for values of the albedo parameter greater than 0.7 (Ref. 20) or 0.09 (Ref. 21).

More recently, analytical and experimental investigations were conducted by Merriam (Ref. 22) on the radiative characteristics of condensed gas deposits on cold surfaces. Absorbing, emitting and scattering media bounded by diffuse and specular surfaces were considered. Effect of different scattering functions were discussed for both gray and non-gray models. The integro-differential transport equation was first integrated. The resulting integral equation was then solved by successive approximation. Results were presented for the reflectance and absorptance of the cryodeposits with diffuse or collimated incident radiation. Since the successive approximation solution of the integral equations would only converge for very low values of the albedo parameter,

comparison between the data and theory was made only for a deposit which was essentially non-scattering. The agreement was reasonable. The method of discrete coordinate was then used (Ref. 22) as a second approach. 24 point single Gaussian quadrature was used and the eigen-values and eigen-vectors were computed by a numerical procedure based on the "method of Danilevsky" quoted in Ref. 23. Solutions for the albedo parameter of 1.0 were obtained to the system of differential equations with all but two of the roots were real and distinct. No comparison was made between theory and experimental data for a highly scattering deposit which corresponds to H_2O and CO_2 cryodeposits in the visible wavelength region.

A different approach was attempted by Wolf (Ref. 24) who treated radiation heat transfer in absorbing, emitting and scattering media with arbitrary temperature profiles in plane, spherical and cylindrical geometries with diffuse bounding surfaces. The transport equation was reduced to a system or ordinary differential equations by using the single Gaussian quadrature in the method of discrete coordinates. The system of equations was then solved numerically by two methods: the modified Euler method and Simpson's rule. Unfortunately, convergence was again not obtained for values of albedo parameter higher than 0.6.

Due to the low temperatures involved, an analysis for a non-emitting cryodeposit has been conducted by Roux (Ref. 25). Absorbing and isotropically scattering media were considered for several types of boundary conditions with either diffuse or collimated radiation incident flux. The solution of the radiation transport equation on a monochromatic basis in the visible wavelength region was

again accomplished by the classical method of discrete coordinates. Single Gaussian quadrature of 10th order was used for the hemispherical-angular reflectance calculations. The system of equations was solved by the Milne predictor-corrector method. The modified Euler method was used as the starting equation for preliminary estimate.

Based on comparisons with experimental results in Ref. 26 and 27, Roux found that the albedo parameter of the deposits was large ($0.9 \leq W \leq 1.0$) in the visible wavelengths region. A limiting value of the hemispherical-angular reflectance (ρ_{ha}) was approached for W less than 0.9 and correspond to the near infrared and infrared wavelength region where CO_2 and H_2O deposits have higher absorption. The following general trends which agree with the experimental data were found in all models investigated:

a) For thin deposits, magnitude of the substrate reflectance has an influence on ρ_{ha}. For very high albedo films the influence is strong and independent of the optical thickness. This influence decreases rapidly for the lower albedo deposits.

b) A reflectance plateau occurred with increasing thickness which was indepentent of the substrate for the more highly absorbing deposits.

c) The reflectance for a cryodeposit on a blank substrate is independent of whether the substrate is assumed diffuse or specular.

It was also found that the angular characteristics of the experimental data was best matched by the model of specular reflector and transmitter on a specular substrate. The numerical solution and the reflectance data of this model were then used to determine the radiative properties σ and α (monochromatic scattering and absorption coefficient) which determine the two governing parameters

t_o and W (optical thickness and albedo) in the analytical results. With known refractive index data, the experimental data of ρ_{ha} at two thicknesses at given view angle were used in conjunction with the solution of the transport equation to solve for σ and α through use of the Newton-Raphson method (Ref. 25). The results were then used to predict ρ_{ha} and intensity profile within the deposits. Although the agreement with the experimental data was good, the analysis was limited to the visible wavelength range only. Based on the study above, the analytical investigation in the present program has been directed in (a) an extension of the analysis to the infrared region and (b) an analysis on cryodeposit with transparent substrate. The effort is being continued in the 1972 Independent-Research program and the results will be included in future reports.

3.3 Previous Experimental Data

Considerable amount of experimental work has been performed during the past decade on thermal radiation properties of cryodeposits. These investigations can be classified into two groups: (a) Calorimetric determination of absorptance and (b) angular and hemispherical spectral reflectance studies. These studies have been made on both monochromatic and total bases using black body sources, mercury-xenon lamps and tungsten-halogen lamps. A summary of previous work done on absorptance measurement is given in table 3 and that on reflectance measurement in Table 4. These works will be considered separately in the following discussions.

3.3.1 Absorptance Studies

The values of absorptance of the cryodeposit-substrate complexes were usually determined calorimetrically on a hemispherical total basis. The sample sur-

TABLE 3 ABSORPTANCE MEASUREMENTS

Investigators	Gas	Surface	Radiation Source	Deposit Thickness mm	Deposition Rate mg/min-cm^2
Moore (Ref. 28)	N_2, CO_2, Air	Cu, 20°K	273°K Blackbody		
Cunningham and Young (Ref. 29)	CO_2	Cu, 77°K	350°K		
	"	Black, 77°K	Blackbody		
Cunningham & Young (Ref. 30)	H_2O	Cu, 77°K	Blackbody		
	"	Black, 77°K	Blackbody		
Caren, et al. (Ref. 31)	CO_2	Al, 77°K	290°K	2.49	1.52
	"	Black, 77°K	Blackbody	3.05	1.52
	H_2O	Al, 77°K	"	.508	.1142
	"	Black, 77°K	"	.508	.1142
	H_2O	Black, 77°K	Hg-Xe lamp	2.79	.1142
Caren, et al. (Ref. 32)	CO_2, N_2 Air	Al, 20°K	70°K Blackbody		
Merriam (Ref. 22)	CO_2	Ni, 78°K	300°K	1.0	
	"	Black, 78°K	Blackbody	1.0	
	H_2O	Ni, 78°K	"	.01	.0053
	"	Black, 78°K	"	.01	"

faces were maintained at cryogenic temperatures and irradiated by blackbody radiation of some characteristic temperature or by radiation from a lamp.

The absorptance of nitrogen, carbon dioxide and water vapor cryodeposits on 20°K copper surfaces for 273°K black body radiation was determined by Moore (Ref. 28). He found that the maximum absorptance obtained with H_2O deposit was 0.9 $\pm$ 0.05 and about two orders of magnitude greater than that of CO_2 or N_2. Cunningham and Young (Ref. 29) measured the absorptance of CO_2 cryodeposits on polished copper and black surfaces irradiated by black body radiation at a characteristic temperature near 350°K. The absorptance increased rapidly with increasing deposit thickness for thin films. At thickness larger than 0.8 mm, an absorptance plateau was reached but the limiting values depended on substrate reflectance. This was attributed to the transparency of solid CO_2 over a large portion of the spectrum.

Caren, et al (Ref. 31) measured the absorptance of CO_2 and H_2O cryodeposits on a polished aluminum surface and a Cat-a-Lac black surface at 77°K with irradiation from a 290°K black body source and from a mercury-xenon lamp. It was also found that the CO_2 is quite transparent to infrared radiation and opacity is not approahced until film thicknesses exceed 2.5 mm. The ice deposit was formed under rarefied-gas condition to obtain an amorphous structure which is representative of that found in an actual space simulation system. (The formation properties of the water deposit is given in the Appendix) . The absorptance of the ice deposit for black body radiation increased gradually and reached a plateau as the thickness exceeded 0.25 mm. The nearly constant value

of 0.91 obtained was essentially independent of the substrate. This agrees with the results reported in Ref. 28 and 30.

When irradiated under a mercury-xenon lamp, the absorptance of H_2O deposit on a Cat-a-Lac black surface decreased gradually as the film thickness increased. When the radiation emitted by the Hg-Xe lamp was filtered to transmit energy only in the solar spectral region, the measured absorptance was even lower. These results indicate that the H_2O deposit is relatively transparent in the visible and very near infrared spectral region.

Results for absorptance for 77°K radiation incident on a 20°K aluminum surface were reported by Caren, et al. in Ref. 32. The condensable gases were CO_2, N_2 and air. The results indicate that these gases in a condensed state are highly transparent to far infrared radiation.

Absorptance of CO_2 and H_2O deposits on polished nickel surfaces and black surfaces at 78°K with irradiation from 300°K blackened chamber wall was measured by Merriam (Ref. 22). The results on CO_2 and H_2O are shown in Fig. 2 and 3 along with results reported in Ref. 29 and 31. There is again the striking difference in results obtained for these two gases. The absorptance values of the highly opaque ice films obtained at thickness larger than 10 microns were already independent of the substrate reflectance. The CO_2 films were more transparent to infrared radiation and the limiting absorptance values were not obtained until the deposit thicknesses reach 1 millimeter. Furthermore, these limiting values for CO_2 film absorptance depended on the substrate reflectance.

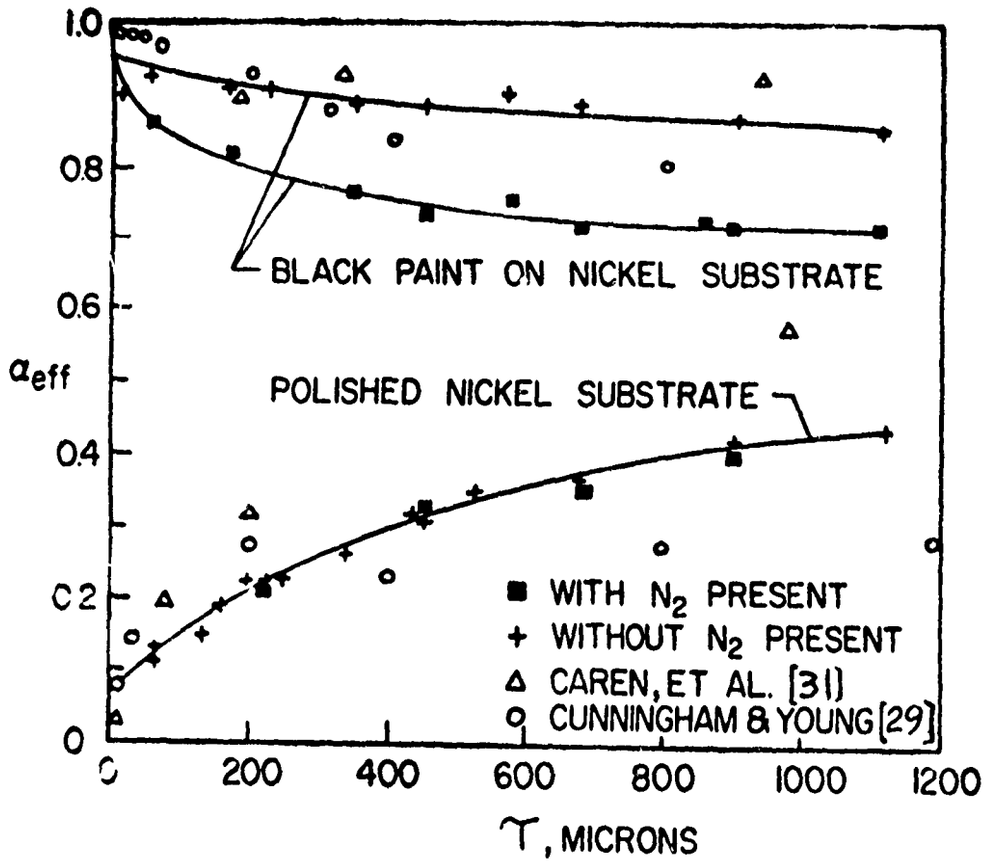

Figure 2. Effective Absorptance of CO_2 Deposits (Ref. 22)

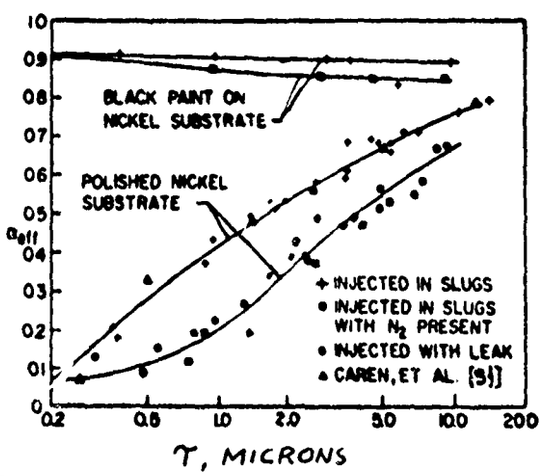

Figure 3. Effective Absorptance of Condensed Water Vapor (Ref. 22)

Studies of the infrared spectral properties of thin CO_2 films have shown that weak absorption bands occur near 2.7, 4.4, 15 and 100 microns (Ref. 22, p. 138) and that CO_2 deposits are highly transparent to infrared radiation. Visual observations by Merrian (Ref. 22) confirmed that the CO_2 deposits were highly scattering. Hence, it is suggested that the attenuation of incident radiation was largely due to scattering.

Results shown in Fig. 3 indicated that the absorptance of a deposit produced from water vapor of high purity* depends significantly on the method of gas injection. When slugs of vapor are injected the deposit is rough and has larger absorptance values that agree with data in Ref. 31. The deposits formed from a slow, steady flow of vapor are smoother and have lower absorptance. In the presence of N_2 gas, the chamber pressure was higher and the shorter mean free path of the slug vapor molecules resulted in more slowly condensation and relatively smoother deposits. This yielded lower absorptance as that obtained by injection with leak.

Visual observations made in both Ref. 31 and 22 indicated that some light scattering occurred in deposits formed from water vapor. Thin deposits appeared

*Pure water was obtained by freezing the water during evacuation of the bottle containing the distilled water, thereby lowering the vapor pressure below 10^{-3} torr.

blue when visible light was incident. The color of the deposit became more nearly white with increasing deposit thickness. At large thicknesses the deposit became very opaque and appeared almost completely white.

3.3.2 Reflectance Studies

Table 4 presents a summary of the various experimental investigations on reflectance measurements. The results are generally given in the forms of hemispherical-angular reflectance ρ_{ha}, angular-hemispherical reflectance ρ_{ah}, and biangular reflectance ρ_{ba}. ρ_{ha} is defined as the ratio of the intensity reflected from an infinitesimal area dA, collected in a specific angular direction θ to the incident intensity which is hemispherically distributed. ρ_{ah} is defined as the ratio of the flux reflected from an infinitesimal element of area dA, collected over the entire hemispherical space to the flux reflected from a white perfectly diffuse-reflecting surface which is a beam oriented at a specific angle ψ relative to the surface normal. ρ_{ba} is defined as the ratio of the intensity reflected from an infinitesimal area dA, collected in a specific angular direction θ to the intensity reflected from a white perfectly diffuse-reflecting surface with the incident radiation a beam oriented at a specific angle ψ. For an isotropic surface with the hemispherically incident intensity diffusely distributed, it can be shown that (Ref. 33)

$$\rho_{ah}(\psi) = \rho_{ha}(\theta) \qquad \text{for } \theta = \psi$$

This equality is of practical importance as the latter is much more readily measured than is the former when the heated cavity reflectometer is used.

TABLE 4. REFLECTANCE MEASUREMENTS

Investigators	Gas	Surface	Radiation Source	Deposit Thickness, mm	Deposition Rate $mg/min\text{-}cm^2$	Wavelength Range, μ	Properties
Wood, et al. (Ref. 34)	CO_2	Stainless Steel, 77°K	W-lamp			0.37 - 0.81	Spectral ρ_{ah} for $\psi = 10°, 30°$ degrees and 45 degrees
	"	Black, 77°K					
Dawson, et al. (Ref. 26)	CO_2	Cu, 77°K	W-I lamp (ρ_{ah})	2.84		0.5 - 1.1	Total ρ_{ah} and ρ_{ba} for $\psi = 0 - 60°$
	"	Black, 77°K	Xe lamp (ρ_{ba})				
McCullough, et al. (Ref. 27)	CO_2	S.S., 77°K	W-I lamp			0.5 - 10	Spectral ρ_{ha}
	"	Black, 77°K					
Wood, et al. (Ref. 35)	CO_2	Cu, 77°K	W-I lamp	1.8	1.44-1.56	.36 - 1.15	Spectral ρ_{ah} for $\psi = 0 - 60°$
	"	Black, 77°K	"	1.8	1.44-1.56	"	
	H_2O	Cu, 77°K	W-I lamp	1.8	.86	.36 - 1.15	
	"	Black, 77°K	W-I lamp	1.32	.6 - .86	"	
Mills & Smith (Ref. 36)	CO_2	Black, 77°K	Xe-lamp	2.51		Simulated Solar	Surface Temperature change
Muller (Ref. 37)	CO_2	Cu, 77°K	Xe-lamp	0.3	.16μ/sec	.7-1.0	ρ_{ba} for $\psi = 11°-66°$
	"	Black, 77°K		0.3	"	"	$\psi = 0°-66°$
	H_2O	Cu, 77°K		0.3	.044 μ/sec	"	$\psi = 11°-55°$
	"	Black, 77°K		0.5	"	"	$\psi = 0°-66°$
Smith, et al. (Ref. 38)	CO_2	Cu, 77°K	Xe-lamp	.27		Visible & Near IR	Total ρ_{ba} $\psi = 0°-70°$ $\delta = -50°$ to 90°
	"	Black, 77°K		.27			
Wood, et al. (Ref. 39)	CO_2	Black, 94°K	Tungsten Halogen lamp	3.38	.336-.36	.5-12	ρ_{ha} for $\delta = 0°-60°$
	"	Stainless Steel 94°K		"	"	"	
Wood, et al. (Ref. 40)	H_2O	Black, 94°K	Tungsten	4.0	.067	.5-12	ρ_{ha} for $\delta = 0°-60°$
	"	Stainless Steel 94°K	Halogen lamp	"	"	"	"

Wood, et al. (Ref. 34) measured the spectral angular-hemispherical reflectance of CO_2 cryodeposits on 77°K black and stainless steel substrates for angle of incidence of 10°, 30° and 45°. It was found that ρ_{ah} decreased as the wavelength increased from 0.37 to 0.81 microns but increased with an increase in the viewing angle θ and an increase in cryodeposit thickness. The dependence of reflectance on angle of incidence became less with increasing deposit thickness.

Dawson, et al. (Ref. 26) measured the total reflectance of CO_2 cryodeposits in the spectral range of 0.5 to 1.1 microns. Angular-hemispherical reflectances were determined by irradiating samples within a vacuum integrating sphere with energy from a tungsten-iodine lamp. A xenon lamp was used for data of biangular reflectances. The surfaces investigated were polished and rough copper, Cat-a-Lac black and a front surface aluminized mirror; all maintained at 77°K. With thin layers of CO_2 deposits, it was found that the total reflectance of the surface is strongly dependent on the reflectance of the substrate. For thick deposits, a reflectance plateau will occur which is essentially independent of the substrate. The reflectance of the surface is also a strong function of the viewing angle of the light reflected. Larger viewing angles (from the surface normal) yield higher total reflectances. Figure 4 illustrates the trend of the angular dependence for a black substrate.

In Ref. 27, measurement of the spectral hemispherical-angular reflectance was extended out to 10 microns wavelength range by the use of a vacuum integrating sphere with powdered sodium chloride coating. Samples were irradiated over the

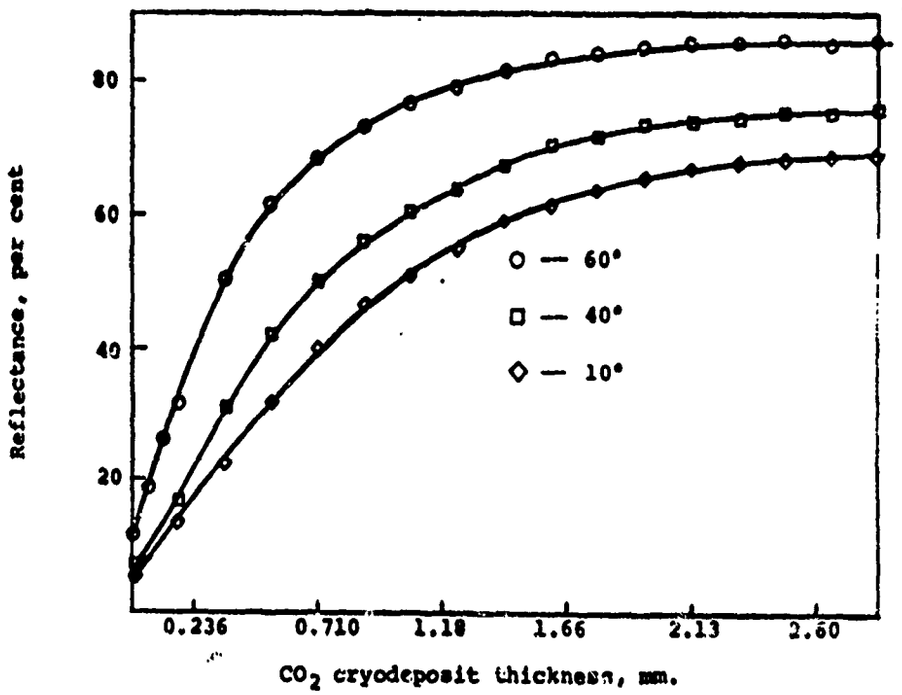

Figure 4. Total angular-hemispherical reflectance of CO_2 cryodeposit on a black paint substrate. (Ref 26)

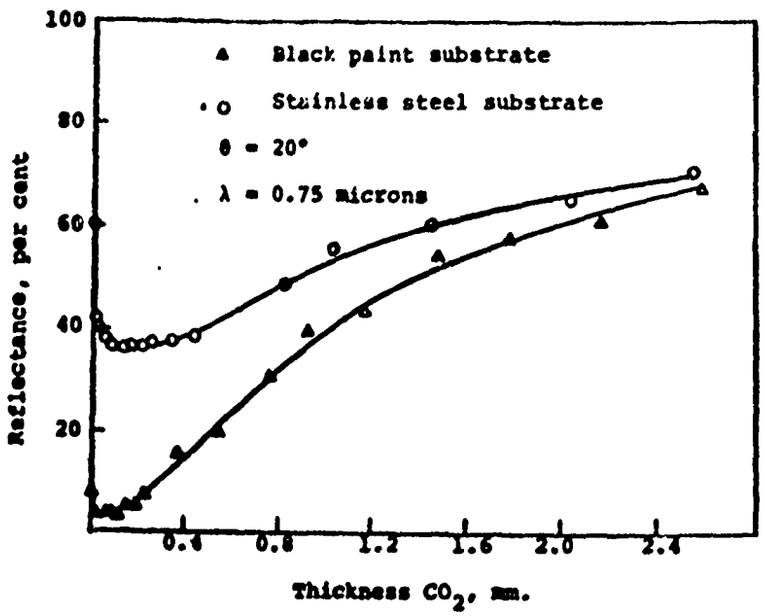

Figure 5. Effect of CO_2 cryodeposit thickness on the cryodeposit-substrate (hemispherical-angular) reflectance.

(Ref 27)

entire hemisphere by monochromatic light from a tungsten-iodine lamp. Reflectance values of CO_2-black paint and CO_2-stainless steel complexes were determined for various angles of incidence. The results as a function of thickness at 0.75 micron are shown in Fig. 5. A sharp reduction in ρ_{ha} is found for very thin CO_2 cryodeposits. With increasing thickness the reflectance attains a minimum and then increase slowly. This is attributed by McCullough, et al. (Ref. 27) to internal scattering and absorption phenomena which occur within the cryodeposit. For large deposit thicknesses, ρ_{ha} of CO_2 deposit is essentially independent of the substrate material. For all thicknesses, however, the reflectance is highly dependent on the wavelength of incident radiation. The results indicate possible absorption bands for CO_2 cryodeposits at 2.7, 4.0, 6.75 and 9.25 microns. Results at these wavelengths show a steady decrease in reflectance with increasing deposit thickness.

Wood, et al. (Ref. 35) concluded from their investigation that the H_2O and CO_2 cryodeposit reflectances on a black paint substrate are strongly dependent on thickness up to approximately 1 mm. A further increase in thickness resulted in a relatively small reflectance change. Thin film interference effects were also observed with polished copper and black paint surfaces. The presence of the thin film of both H_2O and CO_2 caused a decrease in the reflectance corresponds to the sharp initial drop in Figure 5. That this may actually enhance the thermal simulation of space in a vacuum chamber with cryopanels is later confirmed by the experiments conducted by Mills and Smith (Ref. 36) with CO_2 cryodeposits.

Muller (Ref. 37) measured biangular reflectances of CO_2 and H_2O cryodeposits on copper and black paint substrates irradiated by collimated monochromatic beams from a xenon lamp. It was found that as deposit thickness increased, the reflectance in the specular direction decreased but that in the non-specular direction increased. The effect of CO_2 cryodeposit on the angular distribution of visible and near IR radiation reflected from polished copper and black epoxy paint surfaces was further investigated by Smith, et al. (Ref. 38). The results confirmed that the presence of CO_2 deposit causes the incident radiation to be reflected more diffusely. The specular peak in the reflected flux distribution diminishes with increasing CO_2 deposit thickness and at a thickness of 70 microns, it disappears completely for incidence angles less than 70°. Measurements of ρ_{ba} at deposit thickness of 0.27 mm indicate that CO_2 deposit scatter more in the backward direction than in the forward. Off-specular peaks are observed in the angulr distribution of the visible and near IR radiant flux reflected from CO_2 deposits formed on a black substrate for incident angles equal or greater than 50°. Their angular displacement from the specular direction is a function of incidence angle, deposit thickness and deposition rate.

Wood, et al. extended the usable wavelength range of the vacuum integrating sphere used in R f. 27 out to 12.0 micron by using a 1000 w tungsten-halogen lamp as the radiation source. Absolute hemispherical angular reflectances of CO_2 (Ref. 39) and H_2O (Ref. 40) cryodeposits on LN_2-cooled stainless steel substrate, either polished or coated with a black epoxy paint, were determined as functions of substrate material, wavelength λ, deposit thickness τ, deposition rate $\dot{\tau}$, and view angle δ relative to the test surface normal.

The reflectance values measured for CO_2 deposits formed on a black epoxy paint substrate are shown in Fig. 6 for wavelengths between 0.5 and 12.0 microns and a view angle of 10°. By comparison of the data for different thickness, it can be seen that the reflectance begins to increase first at the short wavelengths ($\lambda < 1.5\mu$) and continue to increase for the longer wavelengths as the deposit thickness is increased. For wavelengths greater than 2.0μ, reflectance for very thin deposits is seen to be less than the bare substrate reflectance. This agrees with the results reported in Ref. 35 and 36. The single most prominent spectral feature in the curves of Fig. 6 for thickness less than 0.44 mm is the reflectance peak in the wavelength region of 4.3μ. This peak is attributed to anomalous dispersion (Ref. 25) wherein a strong absorption band in a liquid or solid has associated with it a very high index of refraction so that both absorption and reflection coefficients are quite high. For the 3.38 mm thick deposit the internal scattering has increased significantly which enhances the absorption bands due to the increased reflectance at the nearby wavelengths. The CO_2 deposits were seen to absorb strongly at 2.0, 2.85 and in the vicinity of 4.3μ. Weaker absorption bands were also seen at 3.36, 5.0 and 5.24μ. The reflectance as a function of deposit thickness is given in Fig. 7. It can be seen that thick CO_2 deposits were highly reflecting at the shorter wavelengths ($\lambda < 2.0$).

Reflectance data of CO_2 cryodeposits formed on a stainless steel substrate is given in Fig. 8. An absorption band occurs on the bare polished surface ($\tau = 0$ mm) around 3.0 and the authors (Ref. 39) attributed this to some form of water permanently entrenched in the steel. The absorption bands of CO_2 show up more clearly

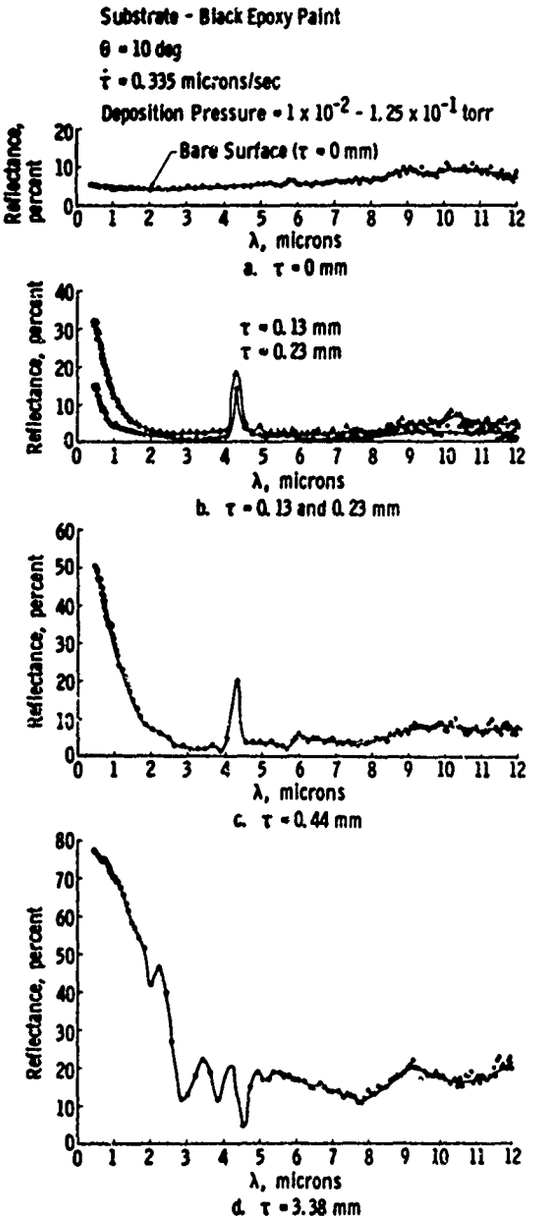

Fig. 6 Reflectance of CO_2 Cryodeposits Formed on a Black Epoxy Paint Substrate (Ref. 39)

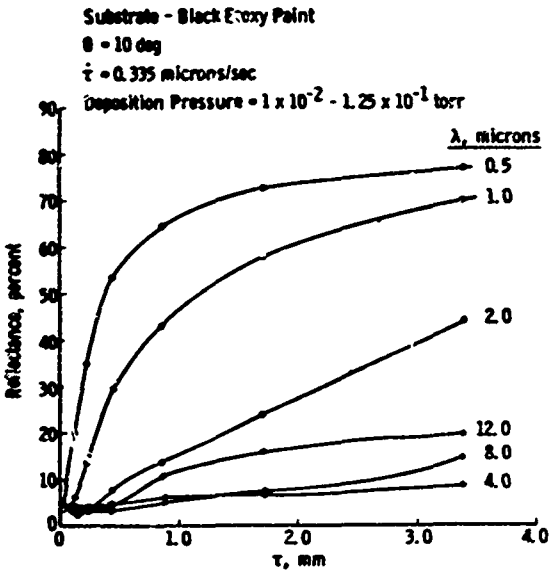

Fig. 7 Reflectance as a Function of Deposit Thickness-Black Paint Substrate (Ref. 39)

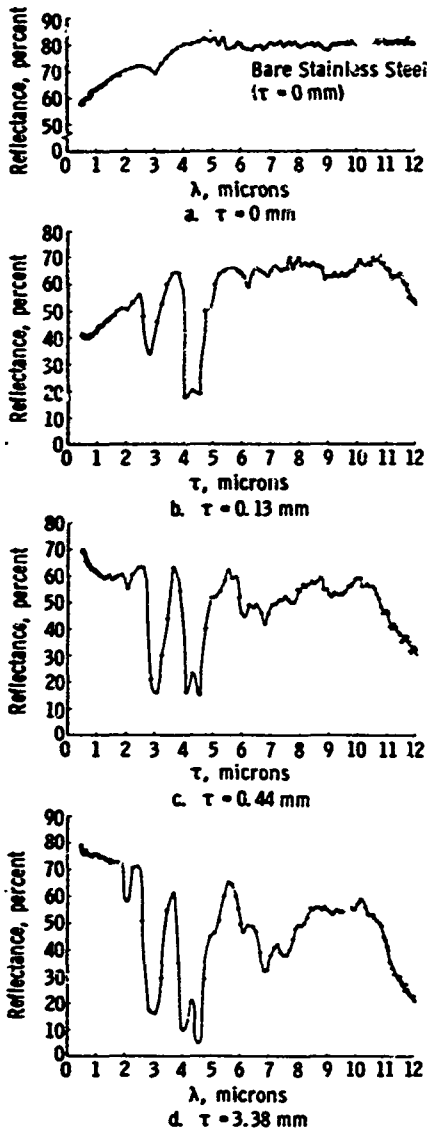

Substrate - Stainless Steel
θ = 10 deg
τ̇ = 0.335 microns/sec
Deposition Pressure = 2 x 10^-2 - 2 x 10^-1 torr

Fig. 8 Reflectance of CO_2 Cryodeposits Formed on a Stainless Steel Substrate (Ref. 39)

in Fig. 8 than in Fig. 6. Absorption bands for the 3.38 mm-thick deposit can be seen to be centered around 2.0, 2.85-3.0, 4.3, 6.1, 6.85 and 7.55μ. By comparing the reflectance data for deposits formed on the two substrates, it can be concluded that thick CO_2 deposits were highly reflecting at the shorter wavelengths ($\lambda < 2.0\mu$) but transmit appreciably at longer wavelengths (excluding absorption bands). It can be argued that if the deposits were not somewhat transparent, the reflectances observed for cryodeposits of equal thickness formed on the two different substrates would be more nearly the same. However, the reflectance at 5.5μ for a 3.88 mm-thick deposit on stainless steel is 65% whereas for an equal thickness on the black substrate the reflectance is only 19%. This indicates that even at this relatively large thickness the substrate reflectance still influences the reflectances of the cryodeposit-substrate complex which can only be explained by the deposit being transparent for radiation at these wavelengths. These results also agree with the observations made in the absorptance tests by Caren, et al. (Ref. 31).

The reflectance was also found to be dependent on view angle for all wavelengths for CO_2 formed on the black epoxy paint. Less dependence on view angle was seen for the deposit formed on the stainless steel substrate.

The amorphous form of water deposits is formed from the vapor in vacuum on surfaces which are 115°K or colder (Ref.43). Absolute hemispherical-angular reflectance of amorphous H_2O cryodeposits formed on a black epoxy paint substrate is presented in Fig. 9. The dependence of reflectance on thickness is shown in Fig. 10. It is seen in Fig. 9 that the reflectance of cold black surfaces

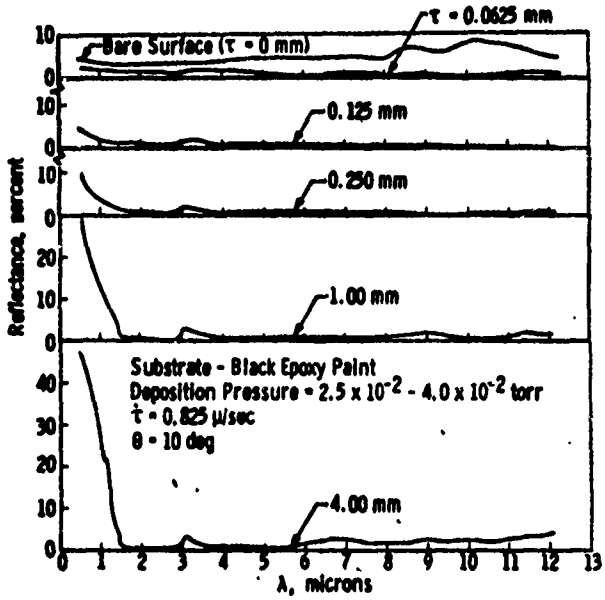

Fig. 9 Spectral reflectance of H_2O cryodeposits formed on a black epoxy paint substrate.

(Ref. 40)

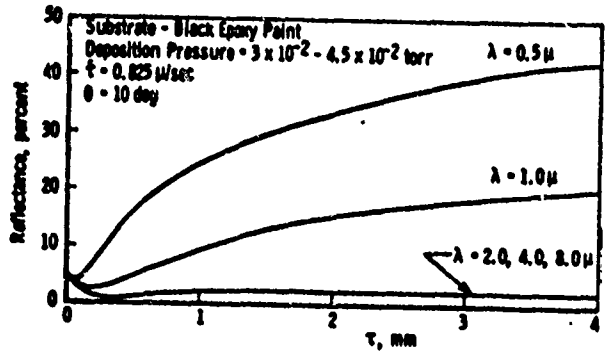

Fig. 10 Dependence of reflectance on thickness for H_2O deposits formed in layers on a black epoxy paint substrate. (Ref. 40)

can be reduced by coating them with a thin solid film of H_2O. In particular, between wavelengths of 2 and 12μ the reflectance can be reduced to 1% or less for an H_2O deposit thickness of 50-100μ. For thickness of H_2O deposit up to 4.0 mm, the reflectance increases almost linearly with decreasing wavelength below about 1.5μ while remains essentially constant at the longer wavelengths. A small anomalous dispersion peak, ceused by the change in refractive index at an absorption band, is observed at wavelengths between 3.1 and 3.25μ. The same effect was observed for CO_2 (Ref. 39). Otherwise, the reflectance in the infrared is essentially independent of thickness and wavelength from $\lambda > 1.5\mu$. In contrast to the CO_2 deposit, the reflectance of the H_2O deposit at large thicknesses is still well below that obtained for the bare black substrate. This indicates that in the infrared, the general trend for amorphous H_2O deposits will be to make absorbing surfaces more absorbing. Fig. 10 shows the gradual increase in reflectance with thickness for the 0.5 and 1.0μ curves. For the other three wavelengths (2.0, 4.0 and 8.0μ), the reflectance is largely independent of both thickness and wavelength. According to results of additional tests, there are no significant differences in the reflectance of deposits formed continuously or in layers. There were also no major reflectance variations with view angle between wavelengths of 0.5 and 8μ.

H_2O deposits formed on the LN_2 cooled polished stainless steel surface reduce the reflectance over the entire wavelength range. As seen in Fig. 11, a deposit of only 30μ thick reduces the reflectance in the infrared from about 75% down to about 15%. This indicates that thin H_2O films can seriously affect the infrared performance of cooled optics. Strong absorption bands occur at 1.55, 2.04, 3.0 and 4.5μ. A broad region of strong absorption

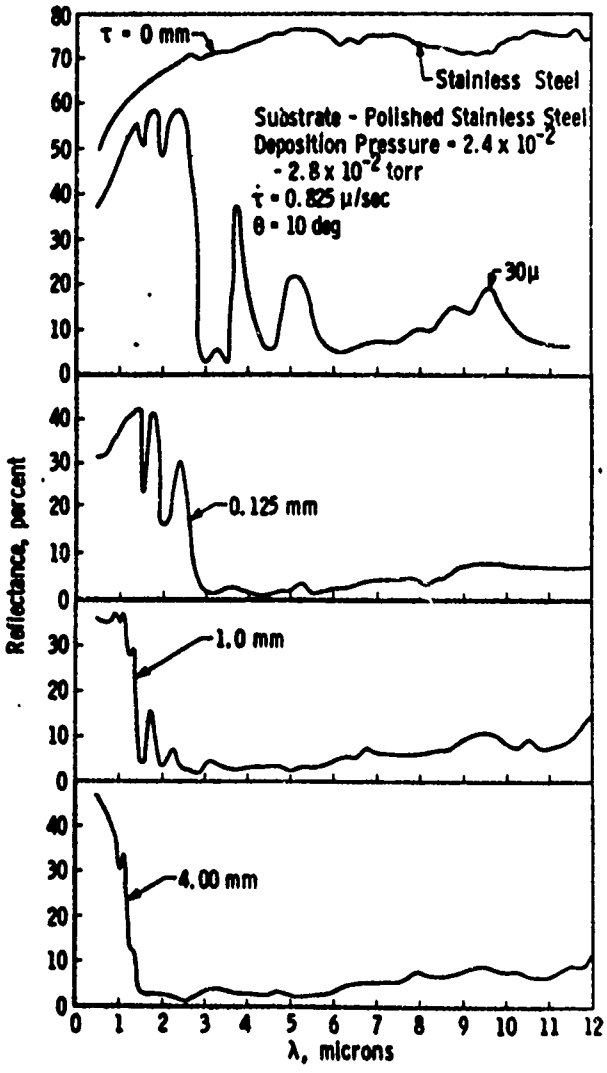

Fig. 11 Spectral reflectance of H_2O cryodeposits formed on a polished stainless steel substrate. (Ref. 4-0)

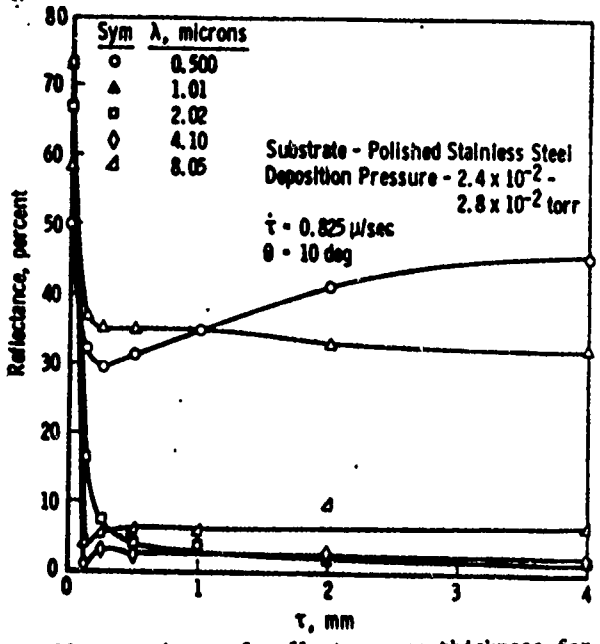

Fig. 12 Dependence of reflectance on thickness for H_2O cryodeposits formed on a polished stainless steel substrate. (Ref. 4-0)

is observed for wavelengths between 3 and 12μ. The wavelength region of strongest absorption appears to be between 3 and 7 μ.

The reflectance variation with H_2O deposit thickness on a stainless steel substrate is shown in Fig. 12. The reflectance at $\lambda = 0.5\mu$ drops from an initial value of 50% down to 30% and then is followed by a gradual rise back to 46% at 4.0 mm thickness. For the other wavelengths, the reflectance is considerably less than the initial value regardless of the deposit thickness.

4. CRYODEPOSITION TESTS

Cryodeposition tests were conducted with a research radiometer (a double focused refractive optical system) in the Research Space Chamber. Controlled amounts of CO_2 and water vapor were introduced as the contaminants which deposited on the LN_2-cooled sun shade and germanium window. Performance of the radiometer sensor system (one Ge:Hg detector and one thermistor bolometer) as determined by the signal attenuation and scattering-interference measured before and after the tests agreed well with previously generated LMSC data (Ref. 31) for solid CO_2 and H_2O absorption.

4.1 Test Apparatus

The LN_2-cooled refractive optical system used to determine the optical degradation resulting from intentional introduction of CO_2 or H_2O gas into the vacuum chamber is shown in Fig. 13. An LHe-cooled Ge:Hg detector was used for most of the CO_2 tests. This was replaced later by a Servotherm thermistor bolometer with KRS-5 window for the remaining CO_2 and H_2O tests. The shade (6) and the optics (1,2) are cooled by liquid nitrogen in tanks (7) and (8).

The radiation source (11) is a blackbody with the temperature maintained at 500°C by a Barnes Model TC-5B temperature controlled. The flux passes through a chopper, a .04-in. aperture and a 8-13μ broadband pass filter. The radiation was modulated at 39 Hz so that the infrared signal reflected from the 8-in. off-axis collimating mirror (10) could be distinguished from stray energy from

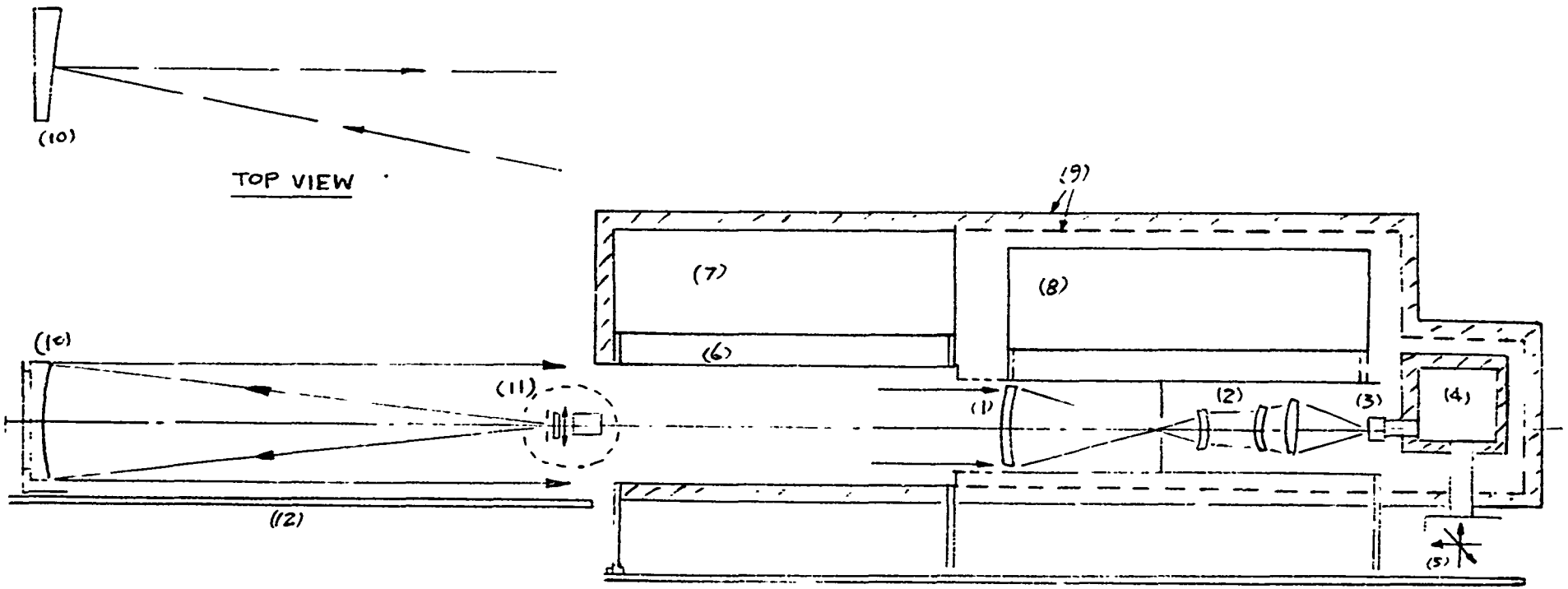

(1) 5-in Diameter Ge Lens
(2) Relay Optics
(3) Detector
(4) LHe Tank
(5) 3-Axis Traverse
(c) Shade
(7) LN_2 for Shade Cooling
(8) LN_2 for Optics Cooling
(9) Shield and Insulation
(10) 8-in Off Axis Collimating Mirror
(11) Aperture, Filter, Chopper & Blackbody Assembly
(12) Collimator 2-Axis Rotary Table

Figure 13. Refractive Optical System 1" = 10"

the surroundings. With the modulated signal and a reference waveform (from a tungsten-lamp illuminated photo cell mounted behind the chopper), it is possible to measure low-level signals using the synchronous technique. A Brower Model 131 Lock-In Voltmeter was used as an AC voltmeter functioning as a high-Q amplifier.

The spectral transmission of the optical system was determined from the spectral reflectance losses on the anti-reflection coated Ge lens and TI-1173 glass and the absorption coefficient data for Ge and TI 1173 glass. The degradation of the system was evaluated from the attenuation of the detector signal output in the 8 to 13 micron wavelength range.

The detector (3) can be positioned and oriented by a 3-axis traversing assembly (5). The radiation source (11) and the mirror (10) are placed on a 2-axis rotary table. This allows the focusing of the radiation flux before and during cooldown of the optical system and measurement of angular distribution of the transmitted radiation flux.

The refractive optical system was placed in the 8-feet diameter search chamber. The glas flow was measured by a Brooks rotameter and passed into the search chamber through a jet made from 1/4-in copper tubings.

4.2 Test Procedure

Due to the large heat capacitance of the LN_2 tanks and the components to be cooled, the search chamber was evacuated down to about 10^{-5} torr the day before the test. The LN_2 tanks and the LHe tank were then filled up with liquid nitrogen and left to stand overnight. On the day of the test, the two LN_2 tanks were again filled up. The LHe tank was first purged with gaseous helium to remove any remaining nitrogen and then filled with liquid helium. When the Ge:Hg detector was cooled down near the LHe temperature, the detector is relocated with the 3-axis transverse (5) to center on the radiation source image. When the thermister bolometer was used in place of the Ge:Hg detector, the LHe was not used. The bolometer was heated instead by a resistor-heater to maintain it at $25^{\circ}C$.

When the detector was centered on the source image, the signal output was at its maximum value. The angular distribution of the transmitted radiation on the detector through a clean Ge window was taken by reading of the detector output while table (12) in Fig. 13 was rotated in the horizontal plane. The table was left at where the detector signal output was again at its maximum value.

The gas was then injected through the chamber wall onto the LN_2-cooled shade and Ge window surfaces. The following quantities were recorded in the duration of gas injection:

Chamber pressure

Gas flow rate

Detector signal output

Temperature at (see Fig. 13)

- LN_2 tank (7)
- LN_2 tank (8)
- Optic shield (9)
- LHe tank (4)
- Shade (6)
- Optics, front (1)
- Optics, rear (2)
- Detector (3)

The temperature of the Ge:Hg detector was measured by the readings of a carbon-resistance thermometer attached to the detector holder. This thermometer was calibrated in the 4° to $30^{\circ}K$ range. The temperature of the thermistor bolometer, as well as the rest of temperatures were measured by chromel- constantan thermocouples. All the temperature measurements were recorded in a Honeywell printer through a Model 707-600 Crossbar Scanner, a Model 620B Digital Multimeter and a Model 824Q Output Control. The chamber pressure as indicated by an ionization gage and the gas flow rate as indicated by the Brooks rotameter were recorded periodically.

The detector signal output was read from the Lock-In Voltmeter and recorded with a Varian Model W-1000 strip-chart recorder. The degradation of the system was first noticed when a steady decrease of the detector output was observed during

normal run conditions. The test was terminated when a nearly constant minimum value was observed over a period of time. The angular distribution of the transmitted radiation on the detector through a contaminated window was then taken for purpose of comparison with the data taken before the gas injection.

Four tests were conducted with CO_2 gas and one test was conducted with H_2O. The test conditions are given in Table 5.

In Tests No. 1 and 2, two LN_2 cooled Granville-Phillips film thickness gages (one exposed and one covered) were placed near the front optical element (the Ge window in Fig.13) to monitor the contamination rate. These quartz crystal gages were not calibrated absolutely at LN_2 temperature and its maximum range is far below the CO_2 thickness required to result in significant attenuation of the detector signal output in present tests. Therefore, no data on the gas deposition rate were obtained and the gages were removed after Test No. 2.

4.3 Test Results

The result of Test No. 1 is given in Fig. 14. When the CO_2 gas was first injected at a flow rate of 1.6 gm/min., an instant rise of the shade temperature and the chamber pressure was observed. Since the jet opening was placed just over the bottom edge of the shade opening and oriented toward the Ge window, this indicated that part of the CO_2 gas molecules deposited on the LN_2-cooled surfaces and the rest reflected from the surfaces. The latter would either

TABLE 5

CRYODEPOSITION TESTS

Test No.	GAS	MAXIMUM FLOW RATE, GM/MIN	INJECTION POINT	DETECTOR	CHAMBER PRESSURE mm Hg
1	CO_2 99.5%	4.35	Bottom edge, Shade opening	Ge:Hg	2 to 8×10^{-5}
2	Ditto	2.3	Top edge, Mirror	"	2×10^{-5} to 4×10^{-4}
3	CO_2 99.99%	1.6	Top and Bottom, Shade Opening	"	10^{-5} to 2×10^{-4}
4	Ditto	6.55	Ditto	Thermistor Bolometer	4×10^{-6} to 1.6×10^{-4}
5	H_2O, Air	6.55	Ditto	"	3.4×10^{-4} to 0.7

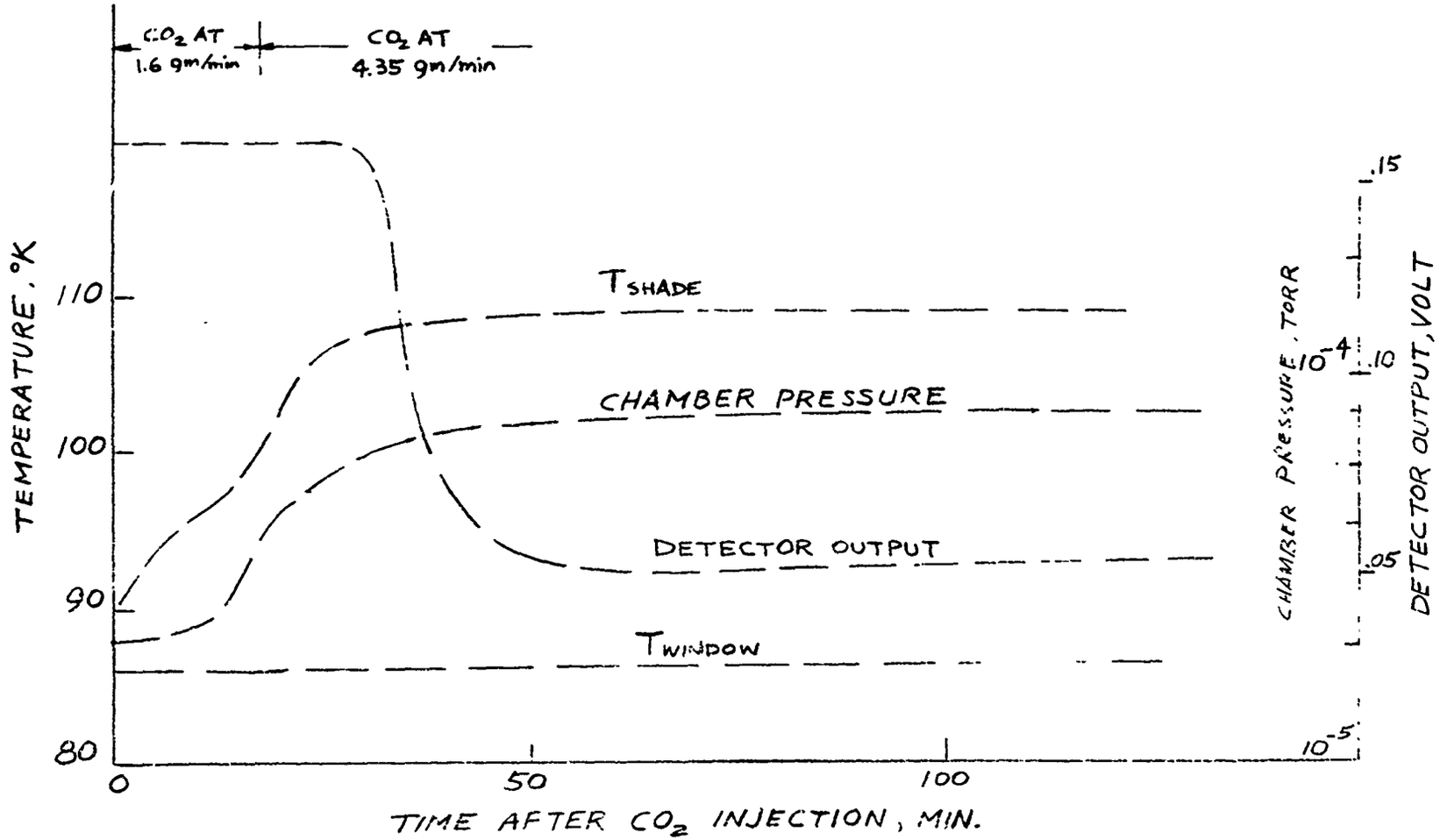

Fig. 14 Cryocontamination test with CO_2 - test No. 1

deposit on the cold surface in succeeding collisions with the cold surfaces or eventually be evacuated from the chamber. The temperature of the Ge windows, which has a much smaller mass than the shade, remained essentially constant and no attenuation of the detector signal output was noticed. After a period of 18 minutes, the CO_2 flow rate was increased to 4.35 gm/min., yielding a more rapid rise in both the shade temperature and the chamber pressure. A rapid attenuation of the detector signal output was observed at about 10 minutes after the change of the CO_2 flow rate. The detector signal output decreased from the original value of 160 mv to 55 mv within a period of 25 minutes. As shown in Fig. 14, continued injection of CO_2 gas failed to cause any further changes in the detector signal outputs.

The results of Test No. 1 as given in Fig. 14 showed qualitative agreement with previous LMSC data on solid CO_2 absorption (Ref. 31) in that the absorption of the deposit-substrate complex also approaches an asymptotic value with deposit thickness (or with time in case of a constant rate of deposition).

When the CO_2 gas flow was shut off, the angular distribution of the transmitted radiation flux on the detector was measured again. The results of the measurement with a clean and a contaminated window were shown in Fig. 15. It can be seen that no significant scattering interference was observed on the angular distribution of the transmitted normal radiation flux in the 8 to 13 micron wavelength range by the presence of CO_2 cryodeposit. This is due to the CO_2 frost scattering which is predominantly at the shorter wavelength region of $\lambda < 1.0\mu$ (Ref. 26, 27).

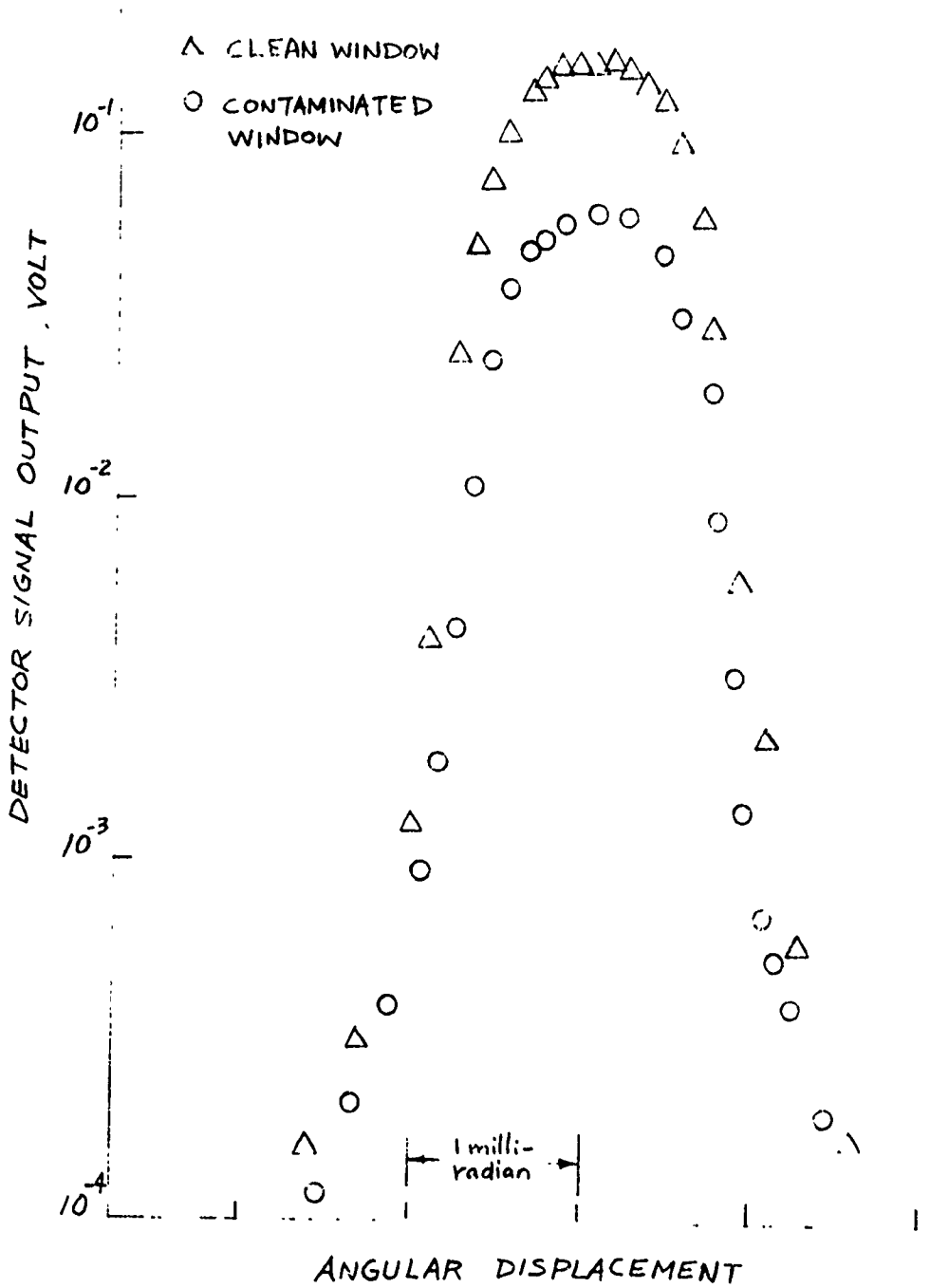

Figure 15. Angular Distribution of Irradiation on Detector

Test No. 2 was conducted under similar conditions except the point of CO_2 injection. This was moved away to just above the collimating mirror, which is located 42 inches from the shade opening. The gas flow began at the rate of 2.3 gm/min which was to be increased gradually until degradation of the optical system was finally observed. However, the chamber pressure increased rapidly from 2×10^{-5} to 3×10^{-4} mm Hg within 3 minutes after gas injection. Hence, no change on the gas flow rate was made during the test. On the other hand, the shade and window temperature as well as the detector signal output remained nearly constant during the 150 minutes of test run. This clearly indicated that the CO_2 gas molecules were removed by the vacuum pump and very few, if any, formed deposit on the LN_2-cooled shade or window surfaces. The mean free path of the CO_2 gas molecules at 3.6×10^{-4} mm Hg is 3.24 inches much smaller than the distance of 42 inches between the jet and the shade opening.

In Test No. 3, the CO_2 gas was metered to two outlets located at the top and bottom edges of the shade opening and oriented toward the Ge window. The flow rate was reduced to 1.6 gm/min to maintain a sufficiently low chamber pressure and a suitable mean free path of the CO_2 gas molecules. With the CO_2 gas injection, the shade temperature increased gradually from 93°K and leveled off at 107°K in 60 minutes. No degradation in performance of the radiometer was detected even though the total amount of CO_2 injected during 150 minutes of test run was twice the amount injected in Test No. 1. It is obvious that the low flow rate created only CO_2 cryodeposition on the shade wall and was not sufficient to cause contamination on the Ge window.

The Ge:Hg detector was replaced by a thermistor bolometer after Test No. 3. In Test No. 4, high purity (99.99%) CO_2 gas was first admitted at 4.35 gm/min. As indicated in Fig. 16, the flow rate was raised to 6.55 gm/min after 100 minutes resulting in a sudden increase in both the chamber pressure and the shade temperature. However, no attenuation of the detector signal output was observed and the CO_2 gas flow was shut off 40 minutes later. Room air was then admitted to the chamber through the same jets at 2.18 gm/min for ten minutes and at 5 gm/min for two more minutes before being shut off. The flow of CO_2 was then started again 14 minutes later at 6.55 gm/min and lasted for 34 minutes. Before the admission of room air, the radiometer performance degraded rather slowly (6% in 140 minutes). The signal output then remained nearly constant until CO_2 was admitted again. This resulted in a loss of signal output from 0.51 mV to 0.25 mV in 16 minutes. The results of tests No. 3 and 4 indicated that the use of a shade sufficiently cooled and maintained at 110°K or lower would protect a cold lens system from typical outgassed amounts of CO_2 for operation in the 8 to 13 microns wavelength range. On the other hand, attenuation of the lens system was accelerated in the presence of impurities. This was evidenced by the results in Test No. 1 where commercial grade CO_2 gas was used and the results in Test No. 4 where high quality pure CO_2 gas and room air were admitted.

A water vapor storage tank with a capacity of 26.9 gallons (101.8 liters) was used in Test No. 5. The tank was evacuated at a pressure equal or lower than the vapor pressure of the distilled water which was stored in a bottle attached to the vapor tank. Unfortunately, a leak was developed in the Brooks rotameter

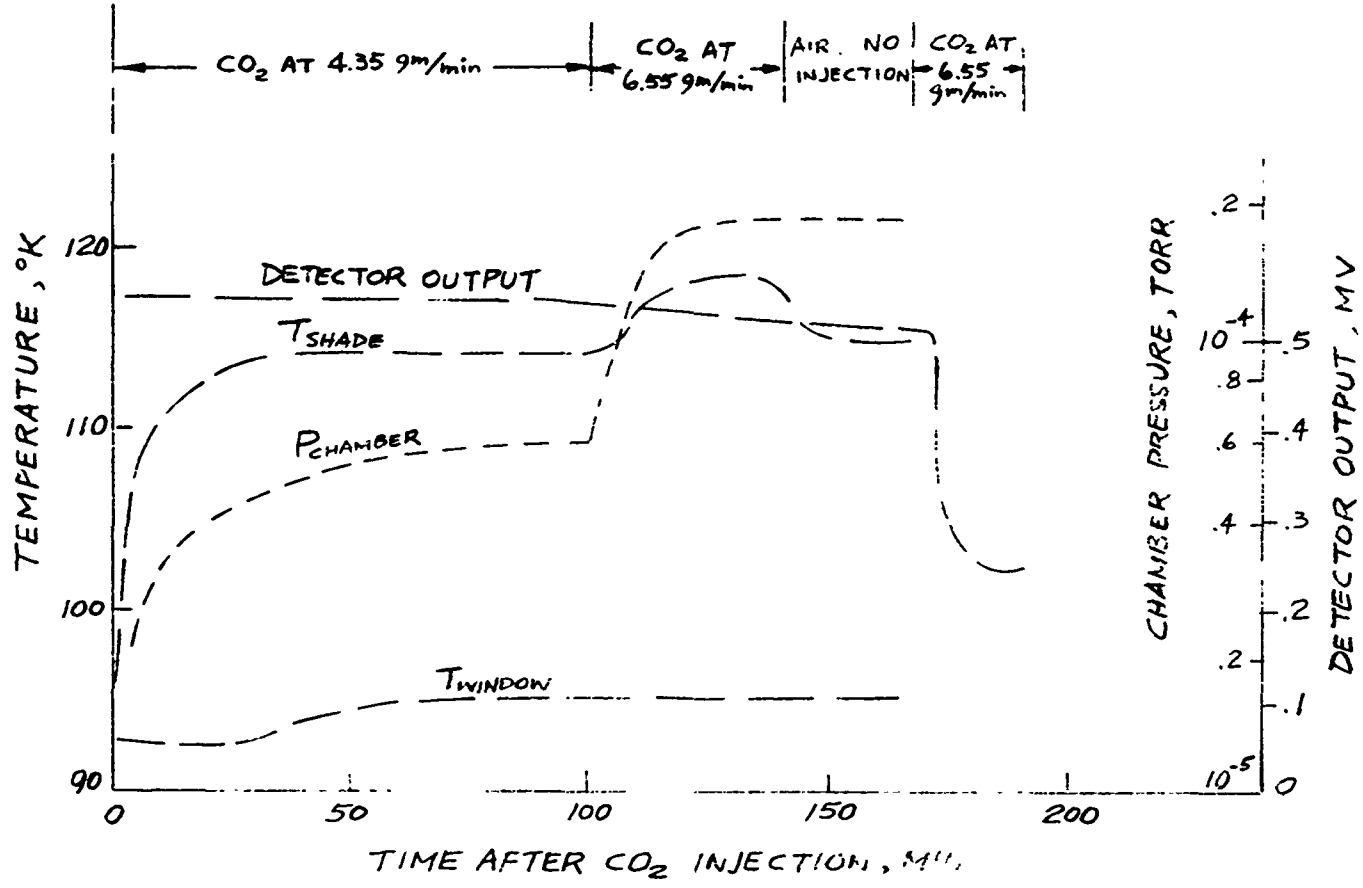

Figure 16. Cryo-Contamination Test with CO_2 Test No. 4 Detector; Thermistor Bolometer

and room air passed into the Search Chamber and the vapor storage tank. Finally, it was decided to admit the room air saturated with water by passing the air through a water container.

The results of Test No. 5 with H_2O saturated room air are presented in Fig. 17. Sensor contamination is evidenced by the attenuation of the thermistor bolometer signal output which was reduced from 0.49 MV to 0.19 MV in 30 minutes. During this period, about 1.78 gm of H_2O vapor contained in the saturated air was introduced. This yielded an estimated H_2O deposit thickness of 0.128 mil based on the density of 0.93 gm/cc for solid H_2O at a pressure of 0.7 mm Hg (Ref. 41, Table 5). Actual values of ice film density would be lower due to the presence of voids in the deposits. Recent measurements reported values of $0.577 \pm .064$ gm/cc (Ref. 31) to $0.81 \pm .02$ gm/cc (Ref. 42). This would indicate a film thickness of 5.27 to 3.74 μ at 30 minutes after air injection.

No sudden change in cryosurface temperatures and accompanying change in signal outputs as expected during change of the ice structure (Ref. 40, Fig. 7) was observed. This indicated that the H_2O deposit remained either in the amorphous form or started with one of the two crystalline forms of ice I, hexagonal (I_h) or cubic (I_c). Based on results summarized in Ref. 43, it can be concluded that the H_2O deposit on the Ge window remained in amorphous form while that on the shade started in the cubic structure.

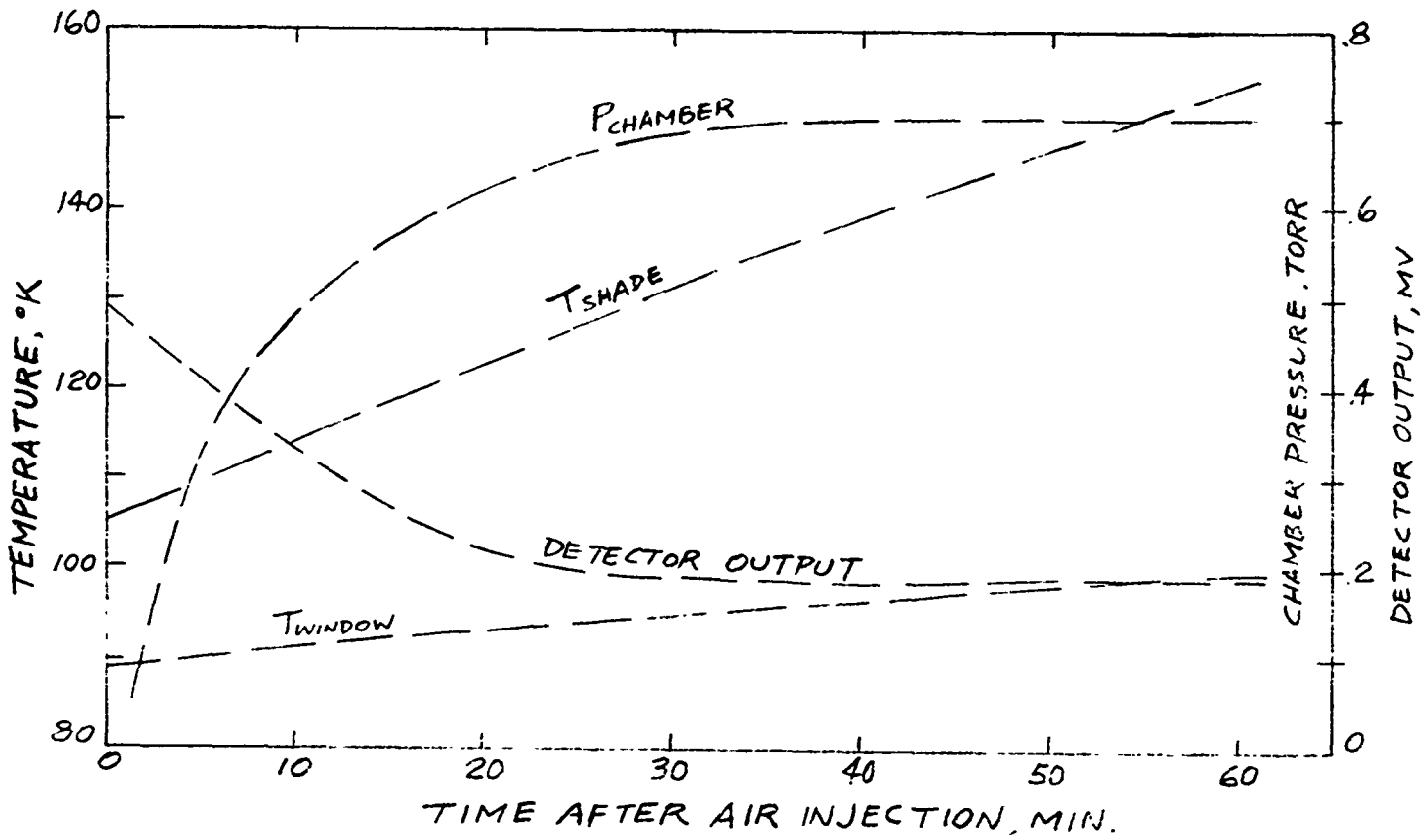

Figure 17. Cryo-Contamination with Air - Test No. 5

5. SUMMARY AND CONCLUSISONS

The investigation was interrupted by change of personnel as well as urgent contractual obligations to be met during the year. However, the following objectives have been achieved in the year 1971:

a. A comprehensive study has been conducted on the possible sources of contaminants that can cause contamination troubles on cooled optical surfaces of a spacecraft. It is concluded that among others, CO_2 and H_2O molecules are most likely to deposit on cold surfaces at the space environment of high vacuum.

b. The radiative characteristics of solid cryodeposit have been studied in detail. The rate of formation of cryodeposits can be calculated when the capture coefficients of given contaminants with respect to the optical surfaces concerned are known. Almost all the analytical works and experimental data on CO_2 and H_2O cryodeposits that have been published up to present date are limited to cryodeposits formed by CO_2 and H_2O on opaque substrate. It is obvious that theoretical and experimental works on transmitting substrate are urgently needed in addition to extending present knowledge on opaque substrates.

c. Cryodeposit tests have been conducted with CO_2 and H_2O-saturated air on LN_2-cooled sunshade and Ge window of a research radiometer in the Search Chamber. Qualitative results from the tests indicated that contamination by CO_2 gas on the LN_2-cooled Ge window (in the 8 to 13 microns wavelength range) can be minimized by a shade maintained at low temperature (below

110°K). However, degradation of the lens system by CO_2 contamination can be accelerated by the presence of impurities. Contamination by H_2O-saturated air occurred at ice film thickness estimated to be less than 5μ. It is concluded that more sophisticated experiments which control and monitor thickness, density, temperature and pressure with spectral transmission measurements are required for additional quantitative data. These experimental results are needed as the physical basis for confirming or disqualifying any future attempt at a realistic mathematical model for the radiative characteristics of solid deposits formed on cryogenic surfaces.

6. REFERENCES

1. McCargo, M., S. A. Greenberg, S. L. McDonald and L. W. Spradley, "Review of the Transient Degradation/Contamination of Thermal Coatings," Final Report, NASA Contract NAS 8-26004, May 1971.
2. Lyon, W. C., "Monopropellant Thruster Exhaust Effects upon Spacecraft," J. Spacecraft and Rockets, Vol. 8, No. 7, July 1971, pp 689-701.
3. Frankel, H. E., "Degradation of the Radiant Cooler of the Nimbus IV High Resolution Infrared Radiometer (HRIR) - Report of the Committee," Memorandum, Oct. 21, 1969, NASA.
4. McNaney, J. J., B. A. Palmer, and R. Shapiro, "Nimbus II Flight Evaluation and Engineering Report, Launch through Orbit 5275 . TN D-4881 Feb. 1969, NASA.
5. McNaney, J. J., "Nimbus III Monthly Flight Evaluation Report Number 1, 14 April to 14 May 1969, Orbits 1 through 400," 69 SD 4295. June 10, 1969, General Electric, Philadelphia, Pa.
6. McNaney, J. J., "Nimbus III Monthly Flight Evaluation Report Number 4, 13 July to 12 August 1969, Orbit 1200 to 1600," 69SD4350, Sept. 10, 1969. General Electric, Philadelphia, Pa.
7. "A Study of Cesium Exhaust from an Ion Engine and its Effect upon Several Spacecraft Components," HIT-399, June 26, 1969, Hittman Associates, Columbia, Md.
8. Lyon, W. C., "A Study of the Effects of Teflon Thruster Exhaust upon a Spacecraft," HIT-443, April 1970, Hittman Associates, Columbia, Md.
9. McPherson, D. G., "Apollo Telescope Mount Extended Applications Study Program, Task IV, A.T.M. Contamination Study," Final Report, NASA CR-61173, Ball Brothers Research Corporation, May 1967.

10. Ratliff, A. W., "Analysis of Exhaust Plumes from Skylab-Configuration R-4D Attitude Control Motors," LMSC/HREC D152171, LMSC Huntsville Research & Engineering Center, Mar. 1970.

11. Handbook of Chemistry & Physics, Chemical Rubber Publishing Co., 42nd ed, 1960 - 1961.

12. Dawson J. P., J. D. Haygood and J. A. Collins, Jr., "Temperature Effects on the Capture Coefficients of CO_2, N and A," Advances in Cryogenic Engineering, Vol. 8, Plenum Press, 1963.

13. Brown, R. F. and E. S. J. Wang, "Capture Coefficients of Gases at 77°K," Advances in Cryogenics Engineering, Vol. 10, Plenum Press, 1965.

14. Levenson, L. L., "Condensation Coefficients of Argon, Krypton, Xenon and Carbon Dioxide Measured with a Quartz Crystal Microbalance," J. Vac. Sci. Technol., Vol. 8, n. 5, 1971.

15. Hobson, J. P., "Physical Adsorption at Extremely Low Pressures," The Solid-Gas Interface, Vol. 1, edited by E. A. Flood, Marcel Dekker, Inc., New York, 1967.

16. Fundamentals of Gas-Surface Interactions, edited by H. Satlsburg, J. N. Smith, Jr. and M. Rogers, Academic Press 1967.

17. Frye, W. E., "Sensor Cryodeposits on Probe Flights," Report LMSC/D246092. Lockheed Palo Alto Research Laboratory, 10 December 1971.

18. Francis, J. E. and T. J. Love, "Radiant Heat Transfer Analys of Isothermal Diathermanous Coatings on a Conductor," AIAA Journal, 4, 643-649, April 1966.

19. Pepper, S. V., "Absorption of Infrared Radiation by Ice Cryodeposits," NASA TN D-5181, April 1969.

20. Hsia, H. M. and T. J. Love, "Radiation Heat Transfer between Parallel Plates Separated by a Nonisothermal Medium with Anisotropic Scattering," Journal of Heat Transfer, C89, 197-203, August 1967.

21. Hottel, H. C., A. F. Sarofim and I. A. Vasolos, "Radiative Transfer in Anisotropically Scattering Media: Allowance for Fresnel Reflection at the Boundaries," Journal of Heat Transfer, C90, 56-62, Feb. 1968.

22. Merriam, R. L., "A Study of Radiative Characteristics of Condensed Gas Deposits on Cold Surfaces," Ph.D. dissertation, Purdue University, June 1968.

23. Faddeva, V. N., Computational Methods of Linear Algebra, Dover Publications, Inc., New York, 1959.

24. Wolf, P., "An Analytical and Experimental Study of the Radiation Heat Transfer in Scattering, Absorbing and Emittang Media," Ph.D. dissertation, The University of Tennessee, Knoxville, Dec. 1968.

25. Roux, J. A., "Radiative Heat Transfer of Coating on a Cryogenic Surface," Ph.D. dissertation, The University of Tennessee, Knoxville, Dec. 1970.

26. Dawson, J. P., B. A. McCullough, B. E. Wood and R. C. Birkebak, "Thermal Radiative Properties of Carbon Dioxide Cryodeposits," Sixth Annual Symposium on Space Environmental Simulation, McDonnel Aircraft Corp., St. Louis, Missouri, 1965. Also Arnold Engineering Development Center Report No. AEDC-TR-65-94, 1965.

27. McCullough, B. A., B. E. Wood, A. M. Smith and R. C. Birkebak, "A Vacuum Integrating Sphere for In Situ Reflectance Measurements at 77°K from 0.5 to 10 Microns," AIAA Paper No. 67-298, 1967.

28. Moore, E. C., "Effect of Gas Condensate on Cryopumps," Transactions of the Ninth National Vacuum Symposium of the American Vacuum Society, The MacMillan Co., New York, 1962, p. 212.

29. Cunningham, T. M. and R. L. Young, "Radiative Properties of Carbon Dioxide Cryodeposits at 77°K," Arnold Engineering Development Center Report No. AEDC-TDR-62-165, 1962.

30. Cunningham, T. M. and R. L. Young, "The Absorptance of Water Cryodeposits at 77°K", Arnold Engineering Development Center Report No. AEDC-TDR-63-155, 1963.

31. Caren, R. P., A. S. Gilcrest and C. A. Zierman, "Thermal Absorptance of Cryodeposits for Solar and 290°K Blackbody Sources," Adv. in Cryo. Engr., Vol. 9, 1964, pp. 457-463.

32. Caren, R. P., A. S. Gilcrest and C. A. Zierman, "An Experimental Determination of the Absorptance of Cryodeposited Film Using Calorimetric Technique", Symposium on Thermal Radiation of Solids, NASA SP-55-1965, pp 531-534.

33. Torrance, K. E. and E. M. Sparrow, Discussion of: Effects of Roughness of Metal Surfaces on Angular Distribution of Monochromatic Radiation, J. Heat Transfer, C87 1965, p.93.

34. Wood, B. E., B. A. McCullough, J. P. Dawson and R. C. Birkebak, "Vacuum Integrating Spheres for Measuring Cryodeposit Reflectances from 0.35 to 15 microns," Arnold Engineering Development Center Report No. AEDC-TR-65-178, 1965.

35. Wood, B. E., A. M. Smith and B. A. Seiber, "Variation of H_2O and CO_2 Cryodeposit Reflectances with Angle of Incidence and Deposit Thickness," Arnold Engineering Development Center Report No. AEDC-TR-68-144, 1968.

36. Mills, D. W. and A. M. Smith,"Effect of Reflections from CO_2 Cryopanel Deposits on the Thermal Balance of a Test Model in a Space Simulation Chamber," J. Spacecraft and Rockets, Vol. 7, Mar. 1970.

37. Muller, P. R., "Measurements of Refractive Index, Density and Reflected Light Distribution for Carbon Dioxide and Water Cryodeposits and also Roughened Glass Surfaces," Ph.D. dissertation, The University of Tennessee, 1969.

38. Smith, A. M., K. E. Templemeyer, P. R. Muller and B. E. Wood,"Angular Distribution of Visible and Near IR Radiation Reflected from CO_2 Cryodeposits," AIAA Journal, Vol. 7, No. 12, 1969.

39. Wood, B. E., A. M. Smith, J. A. Roux and B. A. Seiber, "Spectral Absolute Reflectance of CO_2 Frost from 0.5 to 12.0μ". AIAA Journal, Vol. 9, No. 7, 1971.

40. Wood, B. E., A. M. Smith, J. A. Roux and B. A. Seiber, "Spectral IR Reflectance of H_2O Condensed on LN_2-cooled Surfaces in Vacuum." AIAA Journal, Vol. 9, No. 9, 1971.

41. Kennan, J. H. and F. G. Keyes, Thermodynamic Properties of Steam, John Wiley and Sons, Inc., New York, 31st printing 1958.

42. Seiber, B. A., A. M. Smith, B. E. Wood and P. R. Muller, "Refractive Indices and Densities of H_2O and CO_2 Films Condensed on Cryogenic Surfaces," Applied Optics, 10, 2086-2089, Sept. 1971.

43. Sugisaki, M., H. Suga and S. Seki, "Calorimetric Study of Glass Transition of the Amorphous Ice and of the Phase Transformation Between the Cubic and the Hexagonal Ices," Physics of Ice, Plenum Press, 1969, pp 329-343.

44. Bertie, J. E., L. D. Calvert and E. Whalley, "Transformations of Ice II, Ice III, and Ice V at Atmospheric Pressure," J. of Chemical Physics, 38, 840-846, 1963.

APPENDIX FORMATION PROPERTIES OF WATER DEPOSIT

It has been known that ice formed at various pressures has at least eight crystalline polymorphs of ice, vis., Ice Ih (ordinary hexagonal ice), Ic (cubic Ice I), II, III, IV, V, VI and VII (Ref. 44). Ice formed at pressures of one atmosphere or less is designated as ice I with two crystalline forms (Ih and Ic) and an amorphous form which has no crystalline structure. Table A-1 gives the results summarized in Ref. 43. It appears that water deposits formed at pressure below 5×10^{-3} mm Hg on surfaces that are 115°K or colder will definitely be amorphous. If the surface temperature is between approximately 115°K and 150°K the ice formed will be Ic. For surface temperatures higher than 150°K, the deposit will be Ih. However, these temperatures of formation are not rigid and mixtures of different forms have been observed in the vicinity of the stated temperatures.

The ice deposit can also change structure after it is formed. It can transform from amorphous to cubic to hexagonal but the processes are not reversible. These changes in crystalline forms is usually observed by X-ray diffraction technique. It was found that when the H_2O deposit is warmed up, the amorphous to cubic transition would be observed in the vicinity of 145°K. Transition can occur at lower temperatures but requires longer time period. The Ic to Ih transition was reported to occur between 150°K to 200°K with relatively small heat released. Infrared absorption spectra of the two crystalline forms shows no significant differences. This indicates that the location of the major absorption bands occurs in the same vicinity for both Ic and Ih. Data on the spectral infrared absorption of amorphous ice was reported in Ref. 40.

TABLE A-1 SUMMARY OF PREVIOUS WORK ON ICE STRUCTURES (Ref. 43)

Experimental Method	Temperature Region (°C) -180 -160 -140 -120 -100 -80 -60	Worker
X-ray diffraction	amorphous / semi-crystalline / hexagonal	Burton & Oliver (1935)
thermal analysis	amorphous / crystalline	Staronka (1939)
X-ray diffraction	small crystals + intermediate range not investigated + hexagonal	Vegard & Hillesund (1942)
electron diffraction	small crystals / cubic / hexagonal	Konig (1942)
thermal analysis	amorphous / crystalline	Pryde & Jones (1952)
electron diffraction	crystal growth poor / cubic / hexagonal	Honjo et al. (1956)
thermal analysis	amorphous / crystalline	Ghormley (1956)
thermal analysis	amorphous / crystalline	de Nordwall & Staveley (1956)
electron diffraction	amorphous or small crystals / cubic / hexagonal	Blackman & Lisgarten (1957)
X-ray diffraction	amorphous → cubic → hexagonal	Shallcross & Carpenter (1957)
X-ray diffraction	amorphous / cubic / hexagonal	Dowell & Rinfret (1960)
electron diffraction	halo pattern / cubic → hexagonal	Shimaoka (1960)
X-ray diffraction	amorphous / cubic / hexagonal	Beaumont et al. (1961)
differential thermal analysis	glass / cubic / hexagonal	McMillan & Los (1965)
	supercooled liquid?	
differential thermal analysis	glass	Angell et al. (1967)
thermal expansion	glass	Yannas (1968)
thermal analysis	amorphous / cubic / hexagonal	Ghormley (1968)

This will be presented in the following discussions.

Fig. A-1 gives the temperature and reflectance of H_2O deposit on black substrate measured at a wavelength of 0.55 micron during surface warmup (Ref. 40). Since the transition from amorphous to Ic is exothermic, the temperature increased rapidly from 145°K to about 165°K. The reflectance, which stayed constant until the surface reached the temperature of about 145°K, increased suddently at this instant. Such sudden increase in both the temperature and reflectance of the H_2O deposit is characteristic of transformations from the amorphous to cubic structure. Further warming caused relatively slow conversion of the cubic to hexagonal form with a steady rise in temperature and reflectance. The latter leveled off at about 230 °K.

After the test surface reached 233°K, the surface was again cooled with LN_2 to approximately 100°K. Fig. A-2 shows that the resulting spectral reflectance is greater than that observed for the deposit before warmup by a factor of about 2. Increased internal scattering by the H_2O deposit accentuates the absorption bands at 1.04, 1.25, 1.55, 2.03 and in the vicinity of 2.85 to 3.25 micron. Substantial internal scattering is also seen for the longer wavelengths up to 12.0 micron. No abrupt changes in temperature or reflectance were observed when the test surface was allowed to warm up again. This indicates that the structure changes are irreversible.

Fig. A-3 gives the results on stainless steel obtained after the deposit had been exposed to a dry N_2 pressure of 740 mm hg. The shape and magnitude of

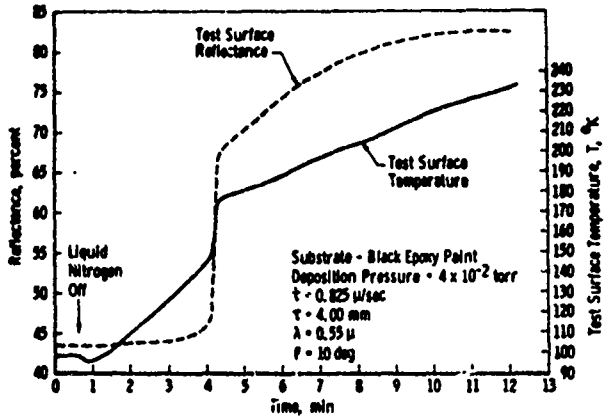

Fig.A-1 Reflectance and temperature variation of H_2O cryodeposit during warmup. (Ref.40)

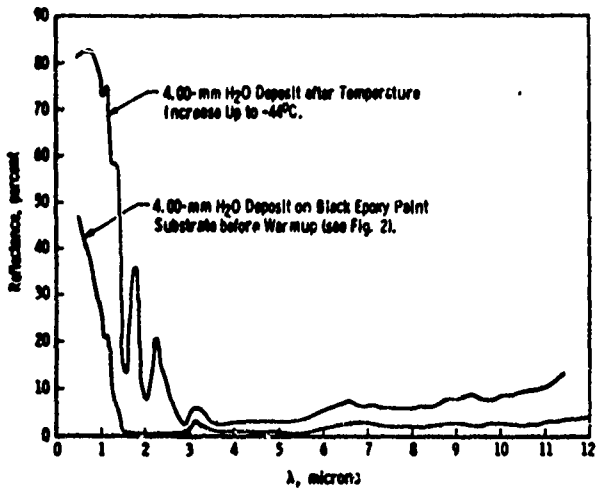

Fig.A-2 Comparison of reflectances of a 4-mm H_2O deposit on black epoxy paint before and after warmup. (Ref.40)

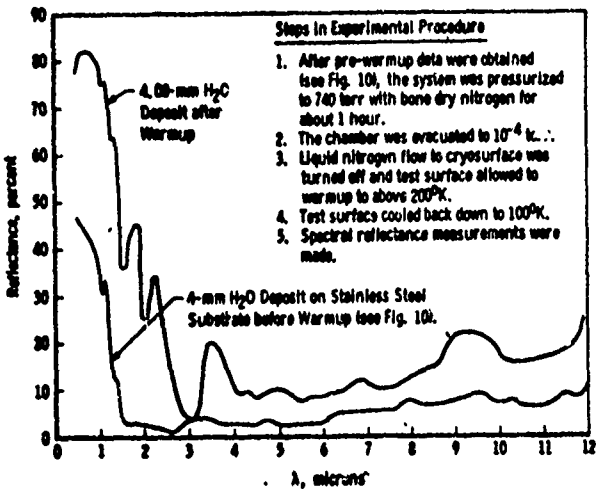

Fig.A-3 Comparison of reflectances of a 4-mm deposit on stainless steel before and after warmup. (Ref.40)

the reflectance curve after warmup is similar to that of the analogous curve in Fig. A-2 with some slight differences. For both cases, absorption bands appear at 1.04, 1.25, 1.55, 2.04 and around 3.0 microns. In Fig. A-3 there is a peak in the reflectance at about 3.5 micron whereas no peak was observed for the annealed deposit on the black substrate in Fig. A-2. This peak at 3.5 micron is suggested in Ref. 40 as not due to scattering alone but also to the increased transmission caused by absorbed N_2 gas in the deposit.